

Clumping Effects in Leaf Area Index Retrieval From Large-Footprint Full-Waveform LiDAR

Hailan Jiang¹, Shiyu Cheng, Guangjian Yan¹, *Senior Member, IEEE*, Andres Kuusk,
Ronghai Hu¹, Yiyi Tong¹, Xihan Mu¹, Donghui Xie¹, Wuming Zhang,
Guoqing Zhou¹, *Senior Member, IEEE*, and Felix Morsdorf²

Abstract—Clumping effect denotes the nonrandomness of foliage. It deviates from the random distribution assumption of Beer’s law which is usually applied to leaf area index (LAI) retrieval from large-footprint full-waveform light detection and ranging (LiDAR). Some studies correct for large gaps-induced between-crown clumping, yet ignore the within-crown clumping. The error of LAI caused by these clumping effects and the influence of the forest structure parameters on them have not been quantitatively studied. This study quantified the between-crown, within-crown, and total clumping indices through a theoretical derivation, clarifying the mechanism of clumping; we used airborne LiDAR point clouds data in 11 290 footprints (diameter = 25 m) to estimate these indices in real forests. We found that: 1) the underestimation of LAI caused by directly applying Beer’s law could be up to 93%, and it decreases with fractional crown coverage but increases with crown length and leaf area density; 2) the method of correcting between-crown clumping improves LAI retrieval for cylindrical canopies effectively; however, 3) considerable underestimation (up to 58%) exists if we neglect the within-crown clumping for other canopies, which has not been realized before; and 4) both the between-crown and the within-crown clumping can be the dominant contributor, and the within-crown clumping was greater than the between-crown clumping in 47% of the studied footprints. In the two physically based LAI retrieval methods, Beer’s law has been commonly used

due to its simplicity. Pathways to improve future LAI retrieval would be instrument improvement to capture the between-crown gaps and method study to correct the within-crown clumping further.

Index Terms—Airborne light detection and ranging (LiDAR), clumping effect, clumping index, full-waveform LiDAR, leaf area index (LAI).

I. INTRODUCTION

LEAF area index (LAI), defined as total one-sided leaf area per unit horizontal ground area [1], [2], is a crucial vegetation structure parameter in the domains of agriculture, forestry, and ecology [2], and is important for modeling mass and energy exchange between the biosphere and the atmosphere [3]–[5]. Light detection and ranging (LiDAR) waveform data quantify the vertical distribution of vegetation by recording highly detailed reflected energy from canopy elements and ground as a function of time (equivalent to the range) [6]–[9]. In the forest that is covered by the footprint (25–70 m, [10]–[12]) of spaceborne LiDAR instruments, such as geoscience laser altimeter system (GLAS) [10] and global ecosystem dynamics investigation (GEDI) [11], the laser pulse emitted by the laser transmitter is capable of reaching the ground through gaps between the foliage elements. Consequently, the saturation problem for a dense forest is minor than that with passive optical remote sensing [6], [11], [13] when using spaceborne LiDAR for LAI retrieval.

The clumping effect denotes the nonrandomness of foliage. In the large footprints of spaceborne LiDAR, real forests generally have heterogeneity at multiple scales. Crowns are dispersed as discrete objects [14], which lead to the between-crown clumping; foliage elements are clumped in the volumes defined by crowns [14], [15], which causes additional within-crown clumping. These phenomena deviate from the random spatial foliage distribution assumption of Beer’s law (gap probability theory) [16]–[20], on which the LAI retrieval from spaceborne LiDAR is based. The clumping of foliage, together with the nonlinear relationship between LAI and gap probability in Beer’s law, usually leads to an underestimation of LAI [21]. In ground-based indirect LAI measurement [2], it might range from 30% to 70% in forests where leaves were highly clumped [22]–[25]. However, less attention has

Manuscript received August 12, 2021; revised September 17, 2021; accepted September 26, 2021. This work was supported in part by the Key Program of the National Natural Science Foundation of China (NSFC) under Grant 42090013 and Grant 41971380, in part by the Guangxi Natural Science Fund for Innovation Research Team under Grant 2019GXNSFGA245001, in part by the University of Zurich Research Priority Program on Global Change and Biodiversity (URPP GCB), and in part by the China Scholarship Council. (*Corresponding author: Guangjian Yan.*)

Hailan Jiang is with the State Key Laboratory of Remote Sensing Science, Faculty of Geographical Science, Beijing Normal University, Beijing 100875, China, and also with the Remote Sensing Laboratories, Department of Geography, University of Zurich, 8057 Zürich, Switzerland.

Shiyu Cheng, Guangjian Yan, Yiyi Tong, Xihan Mu, and Donghui Xie are with the State Key Laboratory of Remote Sensing Science, Faculty of Geographical Science, Beijing Normal University, Beijing 100875, China (e-mail: gjyan@bnu.edu.cn).

Andres Kuusk is with the Tartu Observatory, University of Tartu, Tõravere 61602, Estonia.

Ronghai Hu is with the College of Resources and Environment, University of Chinese Academy of Sciences, Beijing 100049, China.

Wuming Zhang is with the School of Geospatial Engineering and Science, Sun Yat-sen University, Zhuhai 519082, China.

Guoqing Zhou is with the Guangxi Key Laboratory of Spatial Information and Geomatics, Guilin University of Technology, Guilin 532100, China.

Felix Morsdorf is with the Remote Sensing Laboratories, Department of Geography, University of Zurich, 8057 Zürich, Switzerland.

Digital Object Identifier 10.1109/TGRS.2021.3118925

been given to the clumping effect and the impact of forest structure on it in LAI retrieval from a spaceborne LiDAR perspective.

Some of the existing findings in ground LAI measurement could hardly apply to spaceborne LiDAR due to the differences in the measurement setup. They mainly focus on two aspects: 1) in which kind of forest structure the clumping effect is the most severe? and 2) which kind of clumping is the dominant factor influencing LAI retrieval? In LAI retrieval from terrestrial laser scanning (TLS), it was reported that the clumping effect of coniferous plots, on average, is larger than that of the deciduous plots [25]. Ryu *et al.* [26] studied the impact of forest structure on LAI using LAI-2000 Plant Canopy Analyzer (Li-COR, Nebraska, NE, USA). Their results show that the apparent clumping index (i.e., clumping index [1], [17], [27] without considering the shoot-level clumping [15]) is the lowest in canopies with short crown lengths (from the top to the bottom of the crown), large canopy cover, and vertical prolonged crown shape. It indicates that the underestimation of LAI is severe in such cases since the greater the degree of clumping, the smaller the clumping index [26], [28]. However, there is a large difference between TLS, LAI-2000, and spaceborne LiDAR in observing angle: TLS usually observes a hemisphere, LAI-2000 observes beneath the canopy using five central zenith angles ranging from 7° to 68° , and spaceborne LiDAR is placed above the canopy, almost at nadir, with small off-nadir angles (up to 1° for GLAS [29], and up to 6° for GEDI [30]). The conclusions from the ground-based measurements of TLS or LAI-2000 may not be applicable to spaceborne LiDAR since the clumping effect depends on viewing geometry [31]–[35]. In addition, current reports on the dominant factor in the clumping effect are inconsistent so far. For instance, Ryu *et al.* [36] found that the clumping effect is dominant at the between-crown scale in savannas, which corresponds with the open nature of savannas. The study of Hu *et al.* [37] also indicates that between-crown clumping is dominant in their simulated scenes. However, Chen *et al.* [38] found that clumping at shoot level is dominant in boreal coniferous trees. Therefore, the dominant factor depends on the specific forest types and canopy arrangements.

Current physically based methods of LAI retrieval from spaceborne LiDAR either apply Beer's law directly on the total gap probability by assuming the entire footprint as a homogeneous scene [30], [39], [40] or on the gap probability in the crown-covered regions to correct the between-crown clumping [21]. To the best of our knowledge, the clumping in the crown-covered regions has not been considered enough yet. It is important to quantify the clumping effect at different levels, including in the entire footprint, between the crown, and in the crown, so that the mechanism of LAI underestimation and the status of the current methods could be clarified.

The clumping index varies with the radiation pathway [35], making it possible to analyze the clumping effect based on the path length, which denotes the length that the ray passes through a media and is equal everywhere for a homogeneous canopy. The path length distribution model (called PATH) [37]

uses the relative path length distribution, which links the difference in path length with the canopy heterogeneity, to calculate the clumping-corrected "true" LAI from a measured gap probability. Assuming there are functions of the relative path length distribution capable of describing the heterogeneity of different types of the tree crown, a gap probability can be derived from a given true LAI. In addition, by applying Beer's law on this derived gap probability, an effective LAI [41] can be obtained. We aimed to investigate how to theoretically derive the clumping effects based on the definition of the clumping index (i.e., the ratio of the effective LAI and the true LAI). However, the complexity of the real forests makes a theoretical exploration difficult. Following the tradition of using virtual scenes for modeling studies [9], [14], [42], we abstracted the tree crown as a cylinder, sphere (ellipsoid), and cone to characterize crown structures of different forest types. We performed a mathematical derivation of these regular geometries' relative path length distribution functions in the nadir-observing direction of spaceborne LiDAR. We found some general properties of these functions, making a theoretical analysis of the clumping effect possible.

We theoretically investigated how the between-crown, within-crown, and total clumping indices quantitatively change with the influencing factors, including the crown shape, crown length, leaf area density (defined as the one-sided leaf area (m^2) per volumetric unit (m^3) [43]) within the crown, and the fractional crown coverage in the footprint. In addition, we computed these clumping indices from airborne laser scanning (ALS) point clouds data of real forests. Although there is a method of estimating the clumping index from the full-waveform data of GLAS [44], it suffers from the topography effect when the terrain slope is large ($>12^\circ$), and only the total clumping index of the footprint can be obtained. On the contrary, the point clouds data contain more detailed 3-D structure information and are less affected by the topography effect in LAI retrieval when compared with the spaceborne full-waveform data (the topography stretches waveforms, and this effect increases with the terrain slope [45]). We used PATH to compute multiple clumping indices from ALS data [46] within a diameter of 25 m across locations of GEDI footprints in the Canton of Aargau, Switzerland, to have some general knowledge of the clumping effects at large-footprint scale in real forests.

The objective of this study is to explore the following research questions.

- 1) When can Beer's law be applied directly in LAI retrieval without causing large errors?
- 2) What kind of forest structure is suitable for correcting between-crown clumping only?
- 3) How much of the error is caused by either between-crown or within-crown clumping in LAI retrievals? Which kind of clumping effect is the dominant factor in the underestimation of LAI?

Answering the above questions contributes to understanding the mechanism of LAI underestimation caused by clumping effects and providing insights for future improvements of LAI retrievals from large-footprint LiDAR.

II. BACKGROUND

A. Current LAI Retrieval Methods From Large-Footprint Full-Waveform LiDAR Data

1) *Beer's Law*: The traditional Beer's law [16] of light transmission through a turbid medium is used to estimate LAI [30], assuming that the medium of the vegetation is homogeneous in the footprint

$$P_{\text{footprint}}(\theta) = e^{-G(\theta) \cdot \text{LAI}_c / \cos\theta} \quad (1)$$

$$\text{LAI}_c = -\frac{1}{G(\theta)} \cdot \ln(P_{\text{footprint}}(\theta)) \quad (2)$$

where $P_{\text{footprint}}(\theta)$ denotes the gap probability of the footprint in the viewing zenith angle θ ; $G(\theta)$ represents the mean leaf projection coefficient perpendicular to the observing direction and is dependent on the leaf angle distribution and θ . Spherical leaf angle distribution is assumed in this work with a constant 0.5 for $G(\theta)$. Specifically, θ is assumed to be 0° due to the small off-nadir angle of the spaceborne LiDAR. Consequently, we drop $\cos(\theta)$ from (2), and drop θ in the following equations.

2) *Method of Correcting the Between-Crown Clumping*: As the distribution of canopy components is generally not homogeneous, the traditional Beer's law was applied on the gap probability in crown-covered regions (P_{crown} , the probability of the laser beam that shoots toward tree crowns reaching the ground). Then, the retrieved LAI of the crown-covered regions ($\text{LAI}_{\text{crown}}$) by applying Beer's law on P_{crown} was converted to the footprint level using f_{cover} [21]

$$P_{\text{crown}} = \frac{P_{\text{footprint}} - (1 - f_{\text{cover}})}{f_{\text{cover}}} \quad (3)$$

$$\text{LAI}_{e_f_{\text{cover}}} = f_{\text{cover}} \cdot \text{LAI}_{\text{crown}} = f_{\text{cover}} \cdot \left[-\frac{1}{G} \cdot \ln(P_{\text{crown}}) \right] \quad (4)$$

where f_{cover} is the fractional crown coverage within the footprint estimated from the Landsat Thematic Mapper imagery based on the dimidiate pixel model [47] in [21], and $(1 - f_{\text{cover}})$ means the between-crown gap probability (the probability of the laser beam not intersecting with any tree crowns and reaching the ground). Different from the homogeneity assumption across the whole footprint [Fig. 1(b)], this method solved the clumping problem caused by the large gaps [Fig. 1(a)] between crowns in LAI retrieval from GLAS full-waveform data [21].

However, the homogeneity assumption in crown-covered regions indicates that the path lengths of the rays passing through the crown are constant [Fig. 1(c)]. It is usually not the case in real forests [Fig. 1(d)] and leads to an underestimation of the crown LAI ($\text{LAI}_{\text{crown}}$), and thus of the whole footprint LAI, which has not been solved in LAI retrieval from spaceborne LiDAR yet. We will analyze the uncertainty caused by neglecting the clumping in the crown-covered regions, and how the LAI retrieval is improved by correcting the between-crown clumping using the method $\text{LAI}_{e_f_{\text{cover}}}$ [21] in this study.

B. Path Length Distribution Method

PATH was used to characterize variable path lengths through the canopy [see Fig. 1(d)] in the ground and ALS-based LAI

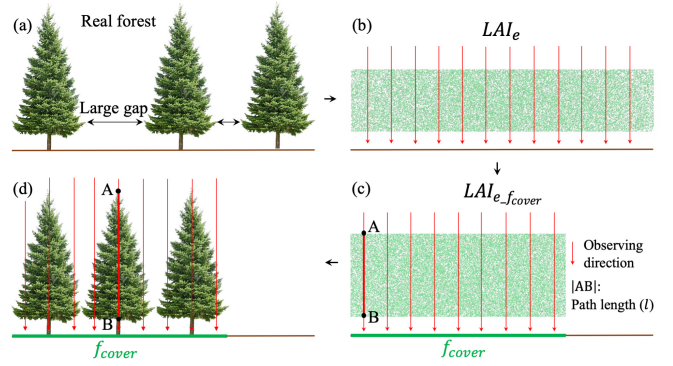


Fig. 1. (a) Real forest, (b) homogeneity assumption in footprint (LAI_e), and (c) crown-covered regions ($\text{LAI}_{e_f_{\text{cover}}}$) in current LAI retrieval methods, and the heterogeneity in the crown-covered regions which can be represented by the difference in path length (d). f_{cover} means the fractional crown coverage, dividing the material in the footprint into two components: vegetation and non-vegetation.

retrieval [37], [46]

$$P_{\text{crown}} = \int_0^1 e^{-G \cdot (\rho \cdot l_{\text{max}}) \cdot l_r} \cdot p(l_r) d(l_r) \quad (5)$$

$$\text{LAI}_{\text{PATH}} = f_{\text{cover}} \cdot \int_0^1 (\rho \cdot l_{\text{max}}) \cdot l_r \cdot p(l_r) d(l_r) \quad (6)$$

where G is the leaf projection coefficient and is assumed to be 0.5, ρ is the leaf area density (unit: m^2/m^3), l is the path length, l_{max} and l_r are the maximum and relative path length ($l_r = l/l_{\text{max}}$), respectively, and $p(l_r)$ is the relative path length distribution function that can characterize the heterogeneity of the canopy, $\int_0^1 p(l_r) d(l_r) = 1$. With known P_{crown} , f_{cover} , $p(l_r)$, and G , $(\rho \cdot l_{\text{max}})$ can be solved from (5); then, the “true LAI”— LAI_{PATH} can be calculated using (6) by substituting $(\rho \cdot l_{\text{max}})$ and $p(l_r)$.

III. METHODS

We computed between-crown, within-crown, and the total clumping index with varying forest structures through a theoretical derivation, and estimated them at the footprints of large-footprint LiDAR scale from real-world data. To be specific, we approximated the forest as abstract canopies composed of regular geometries (representing tree crowns); we assumed the viewing zenith angle to be 0° and the leaf angle distribution [25], [48]–[50] to be spherical. The shoot-level clumping and the woody components [25] were not considered to make the theoretical analysis possible. Furthermore, we used the discrete anisotropic radiative transfer (DART) model [51] to generate various virtual scenes, where exact values of gap probability, LAI, and clumping index are known to test the reliability of the theoretical derivation.

A. Theoretical Derivation of the Clumping Index

Unlike inverting LAI from a known gap probability, we derived the clumping index at crown and footprint level by combining PATH and Beer's law, i.e., from the true LAI to the gap probability, and from the gap probability to the effective LAI. The basis of this derivation is $p(l_r)$ (details about

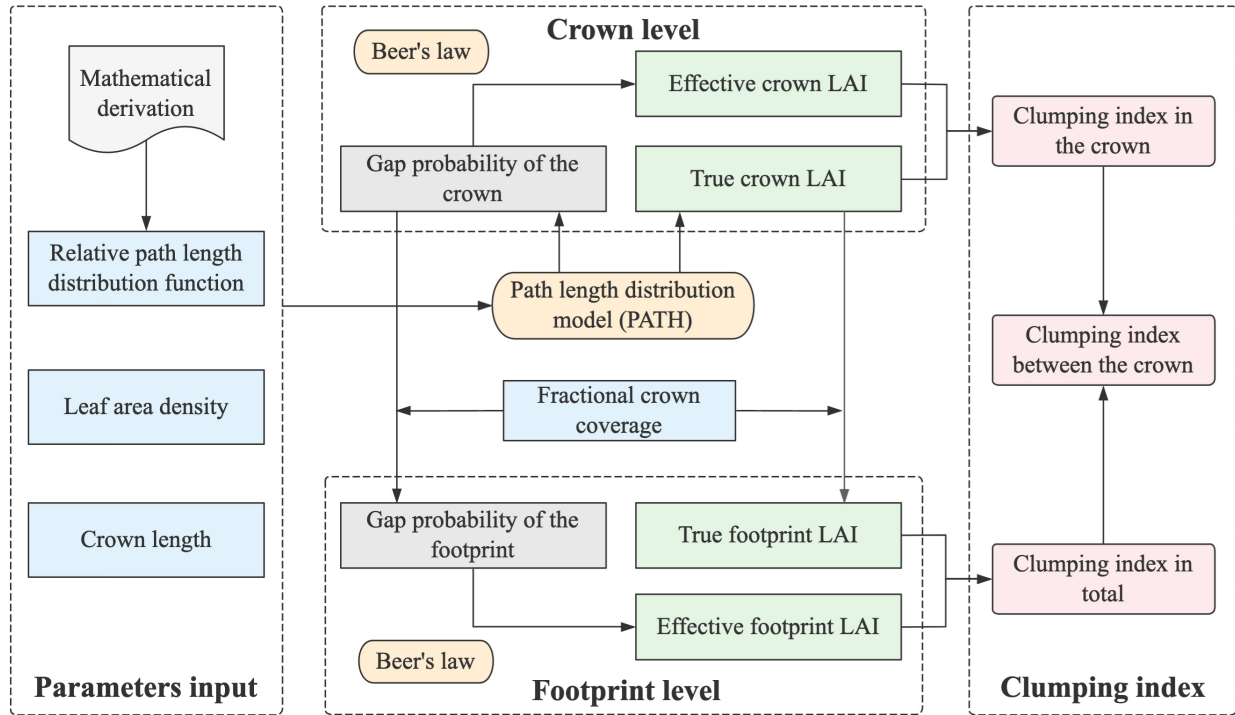


Fig. 2. Workflow diagram for the theoretical derivation of the between-crown, within-crown, and total clumping indices.

the theoretical derivation in Section III-A.1) that is capable of describing the heterogeneity of the crown with different shapes.

The gap probability and true LAI at the crown level were calculated based on PATH with given structure parameters including $p(l_r)$, ρ , and l_{\max} of the regular geometry. Via given f_{cover} , both the gap probability and the true LAI at the crown level were transformed to the footprint level, assuming many of the same geometry were dispersed as discrete objects in the footprint. We obtained the corresponding effective LAI by applying Beer's law on the crown and footprint level gap probability, respectively. Then, we computed the clumping index caused by within-crown clumping (Section III-A.2), within-crown and between-crown clumping together (Section III-A.3), and between-crown clumping (Section III-A.4) for cylindrical, spherical (ellipsoidal), and conical canopies when the viewing zenith angle is 0° . Finally, we identified the dominant factor in the underestimation of LAI (Section III-A.5). Fig. 2 shows the overall derivation process.

1) *Derivation of Relative Path Length Distribution Function of Regular Geometry*: The probability density functions $p(l_r)$ of relative path length (l_r) of regular crowns were derived theoretically, as illustrated in Fig. 3.

For the cylinder, l_r is always 1, so $p(l_r)$ is

$$p(l_r) = \begin{cases} 1, & l_r = 1 \\ 0, & 0 < l_r < 1. \end{cases} \quad (7)$$

For sphere or ellipsoid, the equations of the surface and l_r are

$$\frac{x^2 + y^2}{k^2} + \frac{z^2}{(\frac{1}{2})^2} = 1 (k \neq 0) \quad (8)$$

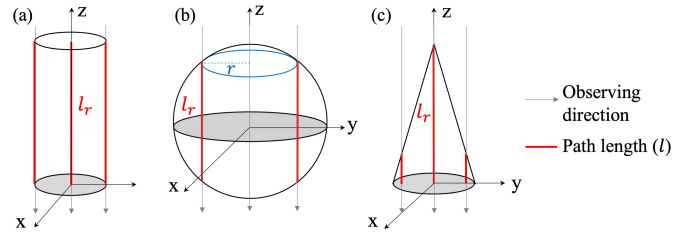


Fig. 3. Schematic of regular geometries [(a) cylinder, (b) sphere, and (c) cone] and (relative) path length (l_r) (red line) that the rays (gray line with arrow) pass through the geometry when the observing zenith angle is 0° . The length (i.e., the maximum path length, l_{\max}) of all the three kinds of geometries is assumed to be 1, so the relative path length (l_r) is equal to the path length (l).

$$l_r = 2|z| \quad (9)$$

where k is a parameter for adjusting the shape of the ellipsoid, being a sphere when $k = 0.5$. Assuming countless rays pass through the sphere with equal lengths (l_r), the intersections with the sphere construct a circle [the blue one in Fig. 3(b)] with a radius of r

$$r^2 = x^2 + y^2 \Rightarrow r = g(l_r) = k\sqrt{1 - l_r^2} (k > 0). \quad (10)$$

Then, the probability density function of r is

$$f(r) = \frac{2r}{k^2} (0 \leq r \leq k). \quad (11)$$

The probability density function of l_r can be given based on (10) and (11)

$$p(l_r) = f(g(l_r)) \cdot |g'(l_r)| = \frac{2k\sqrt{1 - l_r^2}}{k^2} \cdot \left| -\frac{k \cdot l_r}{\sqrt{1 - l_r^2}} \right| = 2l_r (0 < l_r \leq 1). \quad (12)$$

It is noted from (12) that $p(l_r)$ for any sphere or ellipsoid is the same since it is not related to the parameter k .

Similarly, $p(l_r)$ of the cone is not affected by the shape (i.e., whether fat or thin cone) and is

$$p(l_r) = 2 - 2l_r (0 < l_r \leq 1). \quad (13)$$

Therefore, we can use $p(l_r)$ of regular geometries to derive the theoretical error and the clumping effect in corresponding LAI retrieval since the characteristic that $p(l_r)$ is not affected by the length and the specific shape of each kind of geometry makes the theoretical derivation more generally applicable.

2) *Within-Crown Clumping Index*: With theoretical $p(l_r)$ and given ρ and l_{\max} (crown length), we derived the clumping index for a single crown of regular geometry based on its definition, and all the variables related to LAI were defined at the crown level.

Based on the PATH model, the gap probability in the crown area (P_{crown}) for a regular geometry, which is assumed to be filled with randomly distributed leaves with a spherical leaf angle distribution ($G = 0.5$), and a certain ρ , is the weighted average of the transmittance ($T = e^{-G \cdot \rho \cdot l} = e^{-G \cdot (\rho \cdot l_{\max}) \cdot l_r}$) with equal l_r at the crown area, and the weight is $p(l_r)$

$$P_{\text{crown}} = \int_0^1 e^{-G \cdot (\rho \cdot l_{\max}) \cdot l_r} \cdot p(l_r) d(l_r)$$

$$p(l_r) = \begin{cases} 1 (l_r = 1), & \text{Cylinder} \\ 2l_r, & \text{Sphere or ellipsoid} \\ 2 - 2l_r, & \text{Cone.} \end{cases} \quad (14)$$

Based on Beer's law, the effective LAI (LAI_{e_crown}) of the crown is a function of ρ and l_{\max}

$$\text{LAI}_{e_crown} = -\frac{1}{G} \cdot \ln(P_{\text{crown}}) = h(\rho, l_{\max}). \quad (15)$$

The true LAI of the crown ($\text{LAI}_{\text{true_crown}}$) can be calculated from (16) based on the relationship between LAI, ρ , and l ($l_{\max} \cdot l_r$), i.e., LAI of the crown is the weighted average value of LAI_x at locations (x) in the projected area of the crown with the same path length ($l_x = l_{\max} \cdot l_{rx}$), which can be calculated by $\text{LAI}_x = \rho \cdot l_x$, and the weight $p(l_r)$ (derived from Section III-A.1) in (16) is used to consider the nonuniform distribution of l_x (i.e., LAI_x)

$$\text{LAI}_{\text{true_crown}} = \int_0^1 (\rho \cdot l_{\max}) \cdot l_r \cdot p(l_r) d(l_r) = f(\rho, l_{\max})$$

$$= \begin{cases} \rho \cdot l_{\max}, & \text{Cylinder} \\ \frac{2}{3} \cdot \rho \cdot l_{\max}, & \text{Sphere or ellipsoid} \\ \frac{1}{3} \cdot \rho \cdot l_{\max}, & \text{Cone.} \end{cases} \quad (16)$$

The clumping index within the crown is

$$\Omega_{\text{within-crown}} = \frac{\text{LAI}_{e_crown}}{\text{LAI}_{\text{true_crown}}} \quad (17)$$

$\Omega_{\text{within-crown}}$ is a function of leaf area density (ρ) and crown length (l_{\max}), just like LAI_{e_crown} and $\text{LAI}_{\text{true_crown}}$.

Then, the relative error ($\Delta_{\text{within-crown}}$) in LAI_{e_crown} caused by the within-crown clumping is

$$\Delta_{\text{within-crown}} = (\Omega_{\text{within-crown}} - 1) \cdot 100\%. \quad (18)$$

Note that the error caused by within-crown clumping at the footprint level is the same as that for an individual crown if we assume many of the same crowns are dispersed as discrete objects in the footprint, since they share the same $p(l_r)$.

The corresponding relative error of LAI and clumping index in the crown area, caused by within-crown clumping with various crown lengths (1–20 m) and ρ (0.25–1.5), was computed (see Section V-A).

3) *Total Clumping Index*: We calculated the total clumping index at the footprint level by taking f_{cover} into consideration further, assuming many same crowns (with a shape of a cylinder, sphere (ellipsoid), or cone) dispersed as discrete objects in the footprint with f_{cover} ($0.01 \leq f_{\text{cover}} \leq 1$, where 1 indicates closed canopy) and there is no overlapping between them. Similar to those variables for the crown, the corresponding equations at the footprint level are as follows:

$$P_{\text{footprint}} = f_{\text{cover}} \cdot P_{\text{crown}} + (1 - f_{\text{cover}}) \quad (19)$$

$$\text{LAI}_{e_footprint} = -\frac{1}{G} \cdot \ln(P_{\text{footprint}}) = H(\rho, l_{\max}, f_{\text{cover}}) \quad (20)$$

$$\text{LAI}_{\text{true_footprint}} = f_{\text{cover}} \cdot \text{LAI}_{\text{true_crown}}$$

$$= \begin{cases} f_{\text{cover}} \cdot \rho \cdot l_{\max}, & \text{Cylinder} \\ f_{\text{cover}} \cdot \frac{2}{3} \cdot \rho \cdot l_{\max}, & \text{Sphere or ellipsoid} \\ f_{\text{cover}} \cdot \frac{1}{3} \cdot \rho \cdot l_{\max}, & \text{Cone} \end{cases} \quad (21)$$

$$\Omega_{\text{footprint}} = \frac{\text{LAI}_{e_footprint}}{\text{LAI}_{\text{true_footprint}}} \quad (22)$$

$\Omega_{\text{footprint}}$ is caused by within-crown and between-crown clumping together and is a function of leaf area density (ρ), crown length (l_{\max}), and f_{cover} .

The theoretical error of LAI if we directly apply Beer's law on $P_{\text{footprint}}$ is

$$\Delta_{\text{footprint}} = (\Omega_{\text{footprint}} - 1) \cdot 100\% \quad (23)$$

$\Delta_{\text{footprint}}$ and $\Omega_{\text{footprint}}$ with various crown lengths (1–20 m), f_{cover} (0.01–1), and ρ (0.5, 1.0, 1.5), are shown in Section V-C.

4) *Between-Crown Clumping Index*: The total error of the effective LAI at the footprint level is caused by two factors: between-crown clumping and within-crown clumping. The between-crown clumping index is

$$\Omega_{\text{between-crown}} = \frac{\text{LAI}_{e_footprint}}{f_{\text{cover}} \cdot \text{LAI}_{e_crown}} \quad (24)$$

where ($f_{\text{cover}} \cdot \text{LAI}_{e_crown}$) denotes the LAI of the footprint after correcting the between-crown clumping, similar to $\text{LAI}_{e_f_{\text{cover}}}$ in (4). The relative error of LAI caused by the between-crown clumping is

$$\Delta_{\text{between-crown}} = (\Omega_{\text{between-crown}} - 1) \cdot 100\%. \quad (25)$$

Since $\Delta_{\text{between-crown}}$ and $\Omega_{\text{between-crown}}$ are affected by three parameters, we set ρ to be 0.5, 1.0, and 1.5, and the results are shown in Section V-B.

5) *Identification of the Dominant Clumping Effect*: We used the difference between $\Delta_{\text{within-crown}}$ and $\Delta_{\text{between-crown}}$ to judge whether within-crown clumping or between-crown clumping is the dominant contributing factor in LAI underestimation, which is a function of leaf area density (ρ), crown length (l_{max}), and f_{cover}

$$|\Delta_{\text{within-crown}}| - |\Delta_{\text{between-crown}}| = \emptyset(\rho, l_{\text{max}}, f_{\text{cover}}). \quad (26)$$

When $|\Delta_{\text{within-crown}}| - |\Delta_{\text{between-crown}}| > 0$, within-crown clumping is the dominant factor; and when $|\Delta_{\text{within-crown}}| - |\Delta_{\text{between-crown}}| < 0$, between-crown clumping is the dominant contributing factor in LAI underestimation. The results with given ρ (0.5, 1.0, 1.5) for the cylindrical, spherical (ellipsoidal), and conical canopies are shown in Section V-D.

B. Estimation of the Clumping Index From Real-World Data

Although our objective was to quantitatively explore the clumping effect at different scales in LAI retrieval from large-footprint full-waveform LiDAR data, we cannot distinguish them because information of between-crown gaps is lacking in such data. We used ALS point clouds data within the footprints of spaceborne LiDAR—GEDI to quantify them. We retrieved footprint-scale LAIs by correcting different levels of the clumping, including not correcting any clumping (LAI_e), just correcting the between-crown clumping ($\text{LAI}_{e_f_{\text{cover}}}$), and correcting both the between-crown clumping and within-crown clumping (LAI_{PATH}) using the equations above. The related parameters for the retrieval were estimated as follows.

- 1) $P_{\text{footprint}}$ was calculated using an intensity-based method ([52, eq. (14)]) from the point clouds within an off-nadir angle of 10° in the GEDI footprint. This method was reported to be suitable for all footprint sizes of small-footprint ALS, regardless of the structural and optical properties of the vegetation [53]. After the topographic normalization of the original point clouds, a threshold of 3 m was used to further classify the points to forest and nonforest in gap probability calculation; thus, understory with a height less than 3 m was not included in LAIs.
- 2) f_{cover} was estimated from the ratio of the number of pulses whose first returns were classified as vegetation with a height of over 3 m.
- 3) $p(l_r)$ was estimated from the canopy height model (CHM) with a resolution of 0.5 m. Please refer to [46] for more details about the estimation of LAI_{PATH} .

Using LAI_{PATH} as the “true” LAI, we calculated multiple clumping indices according to equations in [46]. The clumping index in total ($\Omega_{\text{footprint}}$), between the crown ($\Omega_{\text{between-crown}}$), and in the crown ($\Omega_{\text{within-crown}}$) was calculated as

$$\Omega_{\text{footprint}} = \text{LAI}_e / \text{LAI}_{\text{PATH}} \quad (27)$$

$$\Omega_{\text{between-crown}} = \text{LAI}_e / \text{LAI}_{e_f_{\text{cover}}} \quad (28)$$

$$\Omega_{\text{within-crown}} = \text{LAI}_{e_f_{\text{cover}}} / \text{LAI}_{\text{PATH}} \quad (29)$$

respectively.

IV. MATERIALS

Virtual scenes with known exact values of gap probability at both the footprint ($P_{\text{footprint}}$) and crown (P_{crown}) levels, f_{cover} , and LAI were generated to test the reliability of the theoretical derivation of the between-crown, within-crown, and total clumping indices, respectively. ALS point clouds data within large footprints of GEDI were used to estimate these kinds of clumping in real forests.

A. Virtual Scenes

We generated abstract discontinuous canopies, where foliage clumps into cylindrical, spherical, and conical tree crown, with three different tree densities (10, 16, and 22 trees, corresponding to f_{cover} values of 0.26, 0.41, and 0.56). Trees were randomly located in the 25-m diameter footprints used by GEDI [11] and the upcoming multifootprint observation LiDAR and imager (MOLI) [12]. To avoid overlap, the distance between the centers of two crowns was larger than the crown diameter (i.e., 4 m). The foliage was constructed using randomly distributed square-shaped scatterers with an area of $0.05 \times 0.05 \text{ m}^2$ (used in [53]). They were located in the cylindrical, spherical, and conical tree crowns on horizontal ground surfaces. The orientations of the leaf elements (scatterers) followed a spherical distribution, i.e., the probability to be intercepted by a leaf were independent of the direction of travel of the radiation, with the leaf projection function G set to be 0.5.

Six different values of ρ (unit: m^2/m^3), ranging from 0.25 to 1.50 with an increment of 0.25, were generated. Notably, 0.25 and 0.5 were used in [53], 0.5 was used in [54], the reported ρ used for broadleaved 3-D crown models summarized by Ligot *et al.* [55] shows that it ranges from 0.3 to 1.32 in seven published studies, and 1.59 was used in [56]. Specifically, we designed the ten cylinders, spheres, and cones with a 4-m diameter, 4-m crown length, and the same locations in the footprint to analyze the clumping effect for the three kinds of regular geometries with the same ρ . We generated 10, 16, and 22 cones, with the diameter at the bottom of the cone of 4 m and length of 8 m, to analyze the clumping effect when ρ , f_{cover} , and the crown length vary in the footprint. Table I provides the detailed properties of the crown and the scatterers for the parameterization in DART, and the geometrical scenes will be shown in Section V.

B. Airborne LiDAR Data

The leaf-on ALS data covering the whole regions of Aargau [Fig. 4(a)] (a canton located in northern Switzerland [Fig. 4(b)] with an area of 1404.4 km^2) were acquired from June 19 to July 15 in 2014 using RIEGL LMS-Q680i long-range laser scanner. The wavelength of the scanner is 1550 nm, and the laser beam divergence is less than 5 mrad (corresponding to about 50-cm increase of beamwidth per 1000-m distance). A maximum number of seven returns were recorded per beam. The operating flight altitude was 700 m, and only data within a $\pm 10^\circ$ scan zenith angle were used to avoid the impact of large off-nadir scan angle on gap probability estimation [57]. The average pulses density is ten pulses per square meter.

TABLE I
PROPERTIES OF THE ABSTRACT DISCONTINUOUS CANOPIES

Abstract discontinuous forest in a 25 m-diameter circular footprint						
Crown geometrical property	Shape	Cylinder	Sphere	Cone		
	Diameter (m)	4	4	4		
	Length (m)	4	4	4-①, 8-②		
	Number (fractional crown coverage)	10 (0.26)	10 (0.26)	10, 16 (0.41), 22 (0.56)		
	Position	Randomly located	Randomly located	Randomly located		
Scatterer property	Shape	Square with an area of $0.05 \times 0.05 \text{ m}^2$ and negligible thickness				
	Leaf normal distribution	Uniform				
Crown structural property	Leaf area density (ρ) (m^2/m^3)	0.25 0.50 0.75 1.00 1.25 1.50	0.25 0.50 0.75 1.00 1.25 1.50	0.25 0.50 0.75 1.00 1.25 1.50		
	Leaf Area Index (LAI) (m^2/m^2)	1.00 2.00 3.00 4.00 5.00 6.00	0.67 1.33 2.00 2.67 3.33 4.00		① 0.33 0.67 1.00 1.33 1.67 2.00	② 0.67 1.33 2.00 2.67 3.33 4.00
					① 0.94 0.89 0.88 0.84 0.80 0.78	② 0.91 0.83 0.77 0.72 0.67 0.63
	Clumping Index (Ω) (0°)	0.96 0.99 0.99 1.01 1.02 1.04	0.95 0.94 0.91 0.90 0.87 0.85			

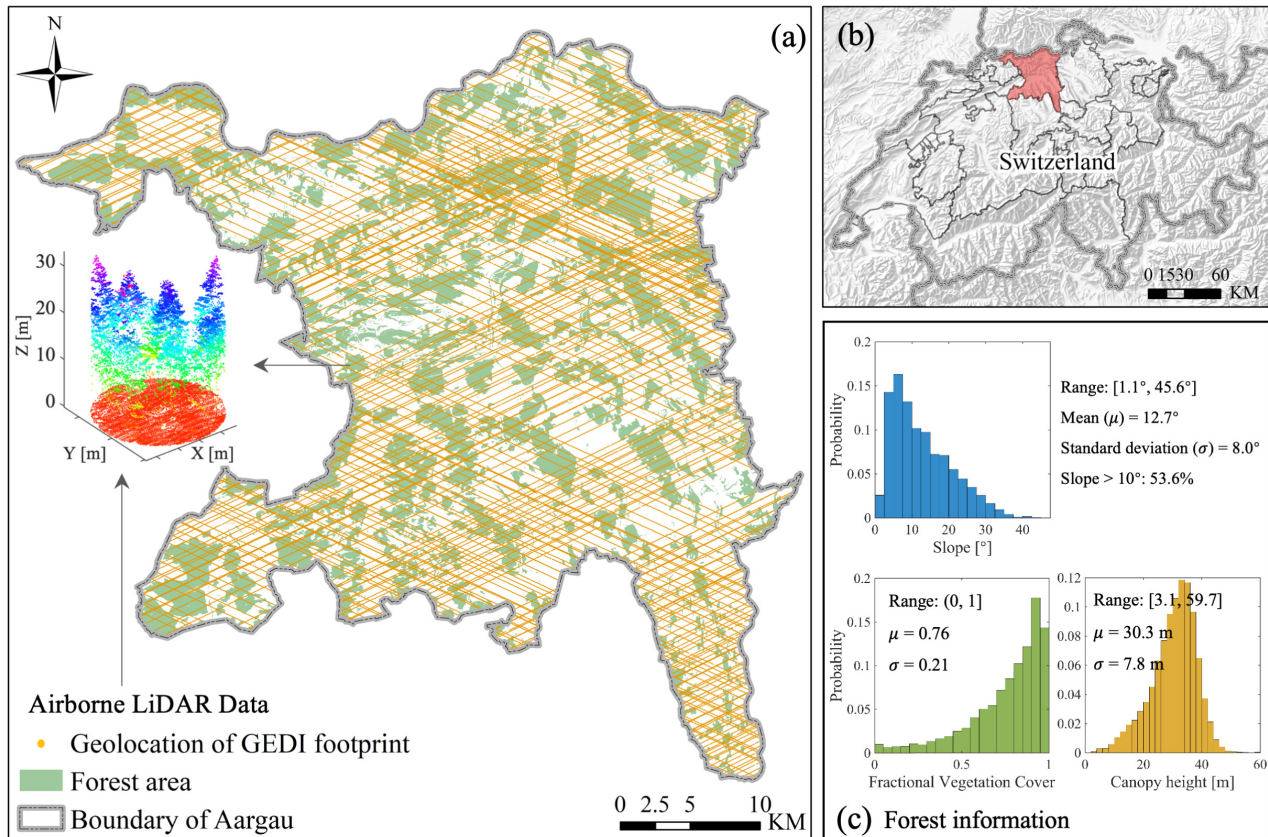


Fig. 4. (a) and (b) Data used in the study area and (c) canopy and topography information computed from ALS data in GEDI-covered footprints in the forest area.

Considering the large data amount, we used the geolocations of GEDI from the GEDI L1B product with the date of data acquisition ranging from April 18, 2019, to April 15, 2020, to sample the ALS point clouds data. We extracted point clouds within each 25-m diameter of GEDI footprint for LAI and clumping index retrieval. The forest and topography information computed from the GEDI-covered footprints in the forest area are shown in Fig. 4(c).

V. RESULTS AND DISCUSSION

For the theoretically derived values, the error caused by the within-crown clumping indicates the theoretical error of method $\text{LAI}_{e_f_cover}$, and error caused by the between-crown clumping and within-crown clumping together indicates the error of method LAI_e ; methods LAI_e and $\text{LAI}_{e_f_cover}$ are the two current physically based LAI retrieval methods from spaceborne full-waveform LiDAR. In addition, the error caused by

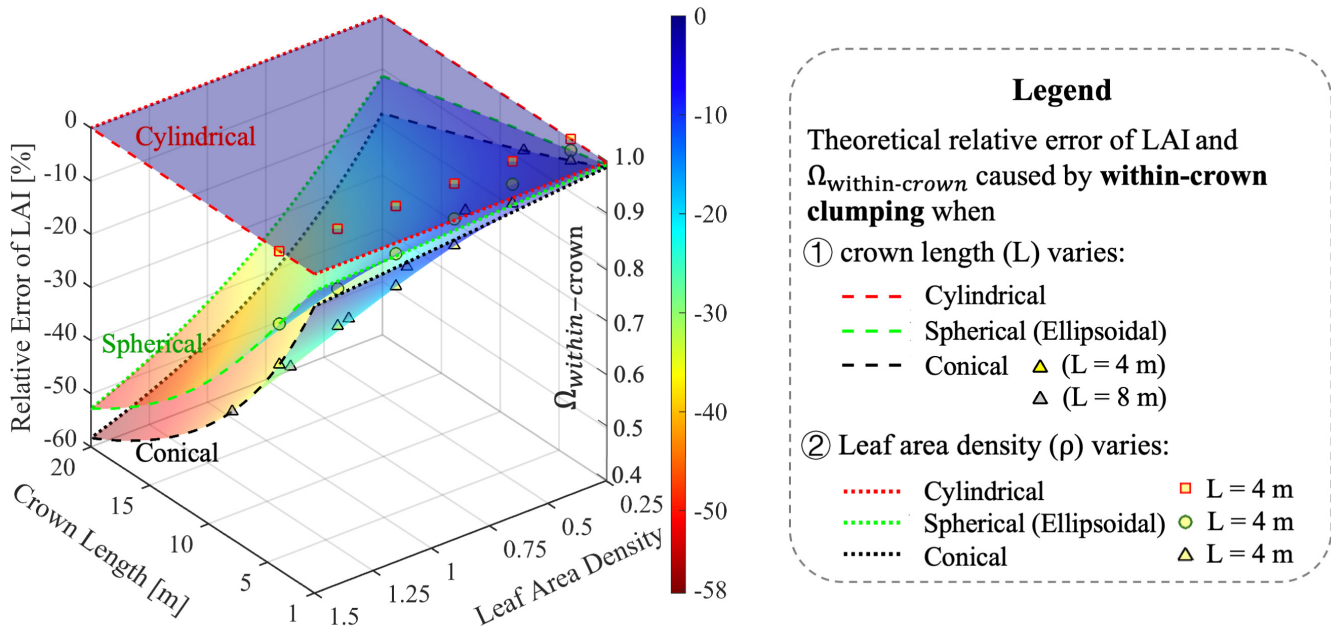


Fig. 5. Theoretical error and clumping index ($\Omega_{\text{within-crown}}$) caused by within-crown clumping in LAI underestimation at various crown lengths and leaf area densities (ρ , unit: m^2/m^3) for cylindrical, spherical (or ellipsoidal), and conical canopies.

the between-crown clumping indicates how much the LAI can be improved by using the method $\text{LAI}_{e_{f_{\text{cover}}}}$.

A. LAI Retrieval Error Caused by Within-Crown Clumping

We theoretically calculated the relative error of LAI and the clumping index ($\Omega_{\text{within-crown}}$) when the viewing zenith angle is 0° in different conditions, including various crown lengths from 1 to 20 m and various ρ from 0.25 to 1.50, caused by within-crown clumping for scenes, which include cylindrical, spherical (ellipsoidal), and conical canopies.

The error caused by within-crown clumping and $\Omega_{\text{within-crown}}$ are a collective effect of crown shape, ρ , and crown length (Fig. 5). Apparently, there is no within-crown clumping for the cylinder since it is a nadir observation. However, for the other kinds of geometry: 1) $|\Delta_{\text{within-crown}}|$ is always larger ($\Omega_{\text{within-crown}}$ is always smaller) for the conical canopy than that for the spherical canopy, due to the greater heterogeneity of the cone in the observing direction and 2) $|\Delta_{\text{within-crown}}|$ increases ($\Omega_{\text{within-crown}}$ decreases) with ρ and crown length. The reason is that the larger the ρ , or the longer the crown, the greater the heterogeneity in the crown area. For instance, it is larger when ρ is 1.5 (6%–58% and 3%–53% for conical and spherical canopies, respectively) than ρ is 0.25 (1%–18% and 1%–11% for conical and spherical canopies, respectively) with crown length ranging from 1 to 20 m. In addition, the theoretical computation is reliable since $\Delta_{\text{within-crown}}$ is nearly consistent with the results of the simulation (Fig. 6 and Table II): $|\Delta_{\text{within-crown}}|$ for the virtual scene simulation and theoretical computation is 22.0% versus 21.4% and 14.7% versus 13.7% for conical and spherical canopies, respectively, when ρ is 1.5 and crown length is 4 m.

Fig. 7 shows the histogram of $\Omega_{\text{within-crown}}$ estimated from the ALS data in 11 290 footprints. $\Omega_{\text{within-crown}}$ ranges

from 0.31 to 1.00 (mean (μ) = 0.89 and the standard deviation (σ) = 0.11).

The error caused by within-crown clumping is seldomly studied from the spaceborne LiDAR perspective. Previous studies on indirect ground-based LAI measurement found a 21%–33% underestimation of the gap size distribution method [37], [58], [59]. Such an underestimation is mainly caused by within-crown clumping [37]. Results from theoretical computation and real-world data show that it could be highly variable (up to 58% underestimation for conical canopies from theoretical derivation, and 0%–69% for the real forests).

B. LAI Retrieval Error Caused by Between-Crown Clumping

The order of error caused by the between-crown clumping ($|\Delta_{\text{between-crown}}|$) is: cylindrical canopy > spherical (ellipsoidal) canopy > conical canopy (Fig. 8), indicating that correcting between-crown clumping is more effective for cylindrical and spherical canopies than that for the conical canopy. Similarly, the order of $\Omega_{\text{between-crown}}$ is: cylindrical canopy < spherical (ellipsoidal) canopy < conical canopy. $\Omega_{\text{between-crown}}$ could be around 0.1 [Fig. 8(c)] at a small f_{cover} (0.01), long crown (20 m), and large ρ ($1.5 \text{ m}^2/\text{m}^3$), indicating that the homogeneity assumption in the footprint will cause larger errors in such cases.

Comparing (a)–(c) in Fig. 8, we found that: 1) $|\Delta_{\text{between-crown}}|$ increases with ρ ; 2) $|\Delta_{\text{between-crown}}|$ increases with the crown length for the cylindrical canopy but not for the spherical (ellipsoidal) and conical canopies; 3) $|\Delta_{\text{between-crown}}|$ decreases with increasing f_{cover} ; however, the larger the ρ , the larger the required f_{cover} is to make $|\Delta_{\text{between-crown}}|$ close to 0, if we make a comparison when crown ρ is 0.5, 1.0, and 1.5 in (a)–(c) in Fig. 8, respectively.

There is a good consistency between $\Delta_{\text{between-crown}}$ from our theoretical computation and the generated virtual scenes,

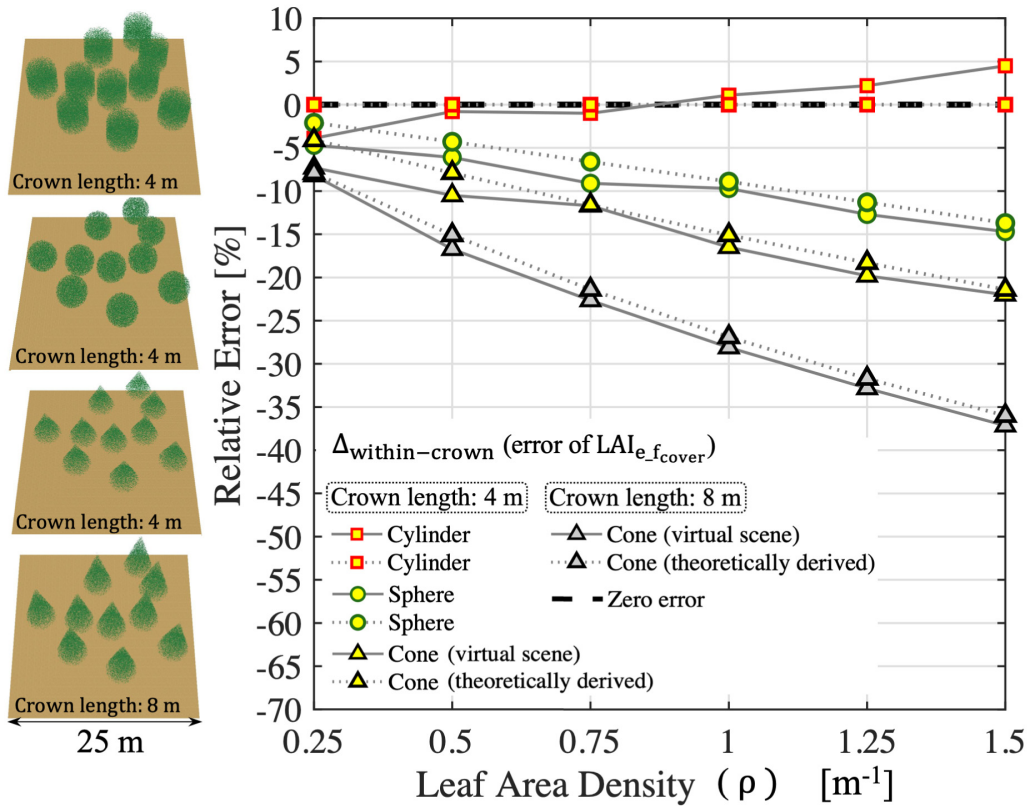


Fig. 6. Geometrical scenes (leaf area density (ρ , unit: m^2/m^3) = 0.75), theoretical relative errors of LAI caused by within-crown clumping [i.e., the errors after correcting the between-crown clumping ($\text{LAI}_{e_{f_{\text{cover}}}}$)] for virtual discontinuous cylindrical, spherical, and conical canopies with the crown ρ ranging from 0.25 to 1.50, and f_{cover} being 0.26.

TABLE II

RELATIVE ERRORS OF LAI CAUSED BY WITHIN-CROWN CLUMPING IN THE FOOTPRINT WITH DIFFERENT CROWN LEAF AREA DENSITY (UNIT: M^2/M^3) AND CROWN SHAPE: FROM THEORETICAL DERIVATION AND THE GENERATED VIRTUAL SCENES

Leaf area density (ρ)	Relative error caused by within-crown clumping (i.e., error of $\text{LAI}_{e_{f_{\text{cover}}}}$)							
	Cylinder (crown length: 4 m)		Sphere (crown length: 4 m)		Cone (crown length: 4 m)		Cone (crown length: 8 m)	
	Virtual scene	Theoretically derived	Virtual scene	Theoretically derived	Virtual scene	Theoretically derived	Virtual scene	Theoretically derived
0.25	-3.9%	0.0%	-4.7%	-2.1%	-7.3%	-4.1%	-8.2%	-7.9%
0.50	-0.8%	0.0%	-6.1%	-4.3%	-10.5%	-7.9%	-16.7%	-15.1%
0.75	-1.0%	0.0%	-9.1%	-6.6%	-11.7%	-11.6%	-22.7%	-21.4%
1.00	1.1%	0.0%	-9.7%	-8.9%	-16.5%	-15.1%	-28.1%	-26.9%
1.25	2.2%	0.0%	-12.7%	-11.3%	-19.8%	-18.3%	-32.8%	-31.7%
1.50	4.5%	0.0%	-14.7%	-13.7%	-22.0%	-21.4%	-37.2%	-36.0%

as shown in Fig. 9 and Table III. In addition, the reliability of the theoretical computation of the clumping indices had only been tested at a 25-m diameter footprint. The findings also suit other footprint sizes as long as multiple tree crowns are included in the footprint. It is because f_{cover} used in the derivation is a relative quantity that combines the coverage of the tree crowns and the size of the footprint.

The histogram of $\Omega_{\text{between-crown}}$ estimated from the real forests is shown in Fig. 10. $\Omega_{\text{between-crown}}$ ranges from 0.29 to 1.00 ($\mu = 0.88$, $\sigma = 0.10$). The average $\Omega_{\text{between-crown}}$ is relatively large, which can partly be explained by the high f_{cover} ($\mu = 0.87$, $\sigma = 0.18$) in the study area. As can be learned from the theoretical derivation (Fig. 8), the larger

the f_{cover} , the smaller the between-crown clumping under the premise that the other structure parameters are fixed.

C. LAI Retrieval Error Caused by Within-Crown and Between-Crown Clumping Together

The theoretical error of effective LAI (LAI_e) and clumping index at footprint scale ($\Omega_{\text{footprint}}$) were calculated by further taking f_{cover} into consideration.

The error of LAI_e is caused by a collective effect of the crown shape, crown length, ρ , and f_{cover} (Fig. 11). Specifically, 1) the trend of the error of LAI_e is exactly opposite to the error caused by within-crown clumping (corresponding to the error of $\text{LAI}_{e_{f_{\text{cover}}}}$) in Fig. 5. The magnitude of error of

TABLE III
RELATIVE ERRORS OF LAI CAUSED BY BETWEEN-CROWN CLUMPING IN THE FOOTPRINT: FROM THEORETICAL DERIVATION AND THE GENERATED VIRTUAL SCENES

Relative error caused by between-crown clumping												
Leaf area density (ρ)	Different crown shape (crown length: 4 m)						Different fractional crown coverage (f_{cover}) (crown length: 8 m)					
	Cylinder ($f_{\text{cover}}: 0.26$)		Sphere ($f_{\text{cover}}: 0.26$)		Cone ($f_{\text{cover}}: 0.26$)		Cone ($f_{\text{cover}}: 0.26$)		Cone ($f_{\text{cover}}: 0.41$)		Cone ($f_{\text{cover}}: 0.56$)	
	Virtual scene	Theoretically derived	Virtual scene	Theoretically derived	Virtual scene	Theoretically derived	Virtual scene	Theoretically derived	Virtual scene	Theoretically derived	Virtual scene	Theoretically derived
0.25	-15.8%	<u>-17.1%</u>	-10.7%	<u>-11.2%</u>	-10.7%	<u>-11.2%</u>	-9.9%	<u>-10.0%</u>	-8.1%	<u>-8.2%</u>	-6.2%	<u>-6.2%</u>
0.50	-30.6%	<u>-31.0%</u>	-19.6%	<u>-20.3%</u>	-19.6%	<u>-20.3%</u>	-15.6%	<u>-16.2%</u>	-13.0%	<u>-13.6%</u>	-10.2%	<u>-10.6%</u>
0.75	-41.5%	<u>-42.3%</u>	-26.1%	<u>-27.4%</u>	-26.1%	<u>-27.4%</u>	-19.4%	<u>-20.0%</u>	-16.5%	<u>-17.0%</u>	-13.0%	<u>-13.6%</u>
1.00	-52.0%	<u>-51.1%</u>	-32.4%	<u>-32.9%</u>	-32.4%	<u>-32.9%</u>	-21.6%	<u>-22.2%</u>	-18.6%	<u>-19.2%</u>	-15.0%	<u>-15.6%</u>
1.25	-60.1%	<u>-58.1%</u>	-36.1%	<u>-37.1%</u>	-36.1%	<u>-37.1%</u>	-22.8%	<u>-23.5%</u>	-19.8%	<u>-20.5%</u>	-16.3%	<u>-16.9%</u>
1.50	-67.9%	<u>-63.7%</u>	-39.4%	<u>-40.2%</u>	-39.4%	<u>-40.2%</u>	-23.3%	<u>-24.1%</u>	-20.5%	<u>-21.2%</u>	-17.0%	<u>-17.7%</u>

TABLE IV
RELATIVE ERRORS OF LAI BY DIRECTLY APPLYING BEER'S LAW IN THE FOOTPRINT: FROM THEORETICAL DERIVATION AND THE GENERATED VIRTUAL SCENES

Relative error caused by between-crown and within-crown clumping (i.e., error of LAI _e of the footprint)												
Leaf area density (ρ)	Different crown shape (crown length: 4 m)						Different fractional crown coverage (f_{cover}) (crown length: 8 m)					
	Cylinder ($f_{\text{cover}}: 0.26$)		Sphere ($f_{\text{cover}}: 0.26$)		Cone ($f_{\text{cover}}: 0.26$)		Cone ($f_{\text{cover}}: 0.26$)		Cone ($f_{\text{cover}}: 0.41$)		Cone ($f_{\text{cover}}: 0.56$)	
	Virtual scene	Theoretically derived	Virtual scene	Theoretically derived	Virtual scene	Theoretically derived	Virtual scene	Theoretically derived	Virtual scene	Theoretically derived	Virtual scene	Theoretically derived
0.25	-19.7%	<u>-17.1%</u>	-15.4%	<u>-13.4%</u>	-12.5%	<u>-9.6%</u>	-18.1%	<u>-17.9%</u>	-16.4%	<u>-16.1%</u>	-14.5%	<u>-14.2%</u>
0.50	-31.4%	<u>-31.0%</u>	-25.7%	<u>-24.6%</u>	-19.9%	<u>-17.9%</u>	-32.3%	<u>-31.3%</u>	-29.9%	<u>-28.6%</u>	-27.0%	<u>-25.7%</u>
0.75	-42.5%	<u>-42.2%</u>	-35.2%	<u>-34.0%</u>	-25.2%	<u>-25.1%</u>	-42.0%	<u>-41.4%</u>	-39.1%	<u>-38.4%</u>	-36.2%	<u>-35.0%</u>
1.00	-50.9%	<u>-51.1%</u>	-42.1%	<u>-41.9%</u>	-32.2%	<u>-31.3%</u>	-49.7%	<u>-49.1%</u>	-46.7%	<u>-46.1%</u>	-43.3%	<u>-42.5%</u>
1.25	-57.9%	<u>-58.1%</u>	-48.8%	<u>-48.4%</u>	-37.5%	<u>-36.7%</u>	-55.6%	<u>-55.2%</u>	-52.8%	<u>-52.2%</u>	-49.3%	<u>-48.6%</u>
1.50	-63.4%	<u>-63.7%</u>	-54.1%	<u>-53.9%</u>	-41.7%	<u>-41.4%</u>	-60.5%	<u>-60.1%</u>	-57.7%	<u>-57.2%</u>	-54.2%	<u>-53.7%</u>

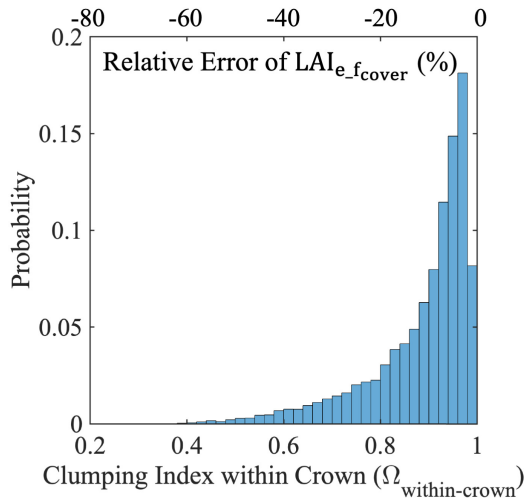


Fig. 7. Histogram of the within-crown clumping index ($\Omega_{\text{within-crown}}$) estimated from ALS point clouds data in 11 290 footprints with a diameter of 25 m. $\text{LAI}_{e_f_{\text{cover}}}$ denotes the retrieved LAI by correcting the between-crown clumping.

LAI_e is: cylindrical canopy > spherical (ellipsoidal) canopy > conical canopy, due to the considerable heterogeneity resulting from the large gaps between crowns for a cylindrical canopy. It indicates that the clumping effect at the footprint scale is most serious in open cylindrical canopies; 2) the error of LAI_e

increases ($\Omega_{\text{footprint}}$ decreases) with crown ρ (ρ changes from 0.5 to 1.5 with an increment of 0.5 in Fig. 11), since the larger the crown ρ , the greater the heterogeneity in the footprint; 3) errors of LAI_e and $\text{LAI}_{e_f_{\text{cover}}}$ (the error in Fig. 11 when $f_{\text{cover}} = 1$) increase with the crown length since the longer the crown, the greater the heterogeneity in the footprint scale for LAI_e and crown area for $\text{LAI}_{e_f_{\text{cover}}}$ retrieval; and 4) error of LAI_e decreases ($\Omega_{\text{footprint}}$ increases) with increasing f_{cover} since the larger the f_{cover} , the closer the scene is to a homogeneous distribution of canopy elements. These computations are consistent with those of our generated virtual scenes in Fig. 12 and Table IV. Moreover, when f_{cover} is 1 in Fig. 11, the error is only caused by within-crown clumping.

There is a large difference between the clumping index at the crown level and the footprint level. Comparing $\Omega_{\text{footprint}}$ (Fig. 11) and $\Omega_{\text{within-crown}}$ (Fig. 5), $\Omega_{\text{within-crown}}$ is 1 for the cylindrical crown, but $\Omega_{\text{footprint}}$ for the cylindrical canopy could be around 0.1 at a small f_{cover} (0.01), long crown (20 m), and large ρ (1.5). It indicates that we are unable to know $\Omega_{\text{footprint}}$ even though we know $\Omega_{\text{within-crown}}$ for a specific tree in advance due to the large impact of the between-crown gaps in the footprint. In addition, the large difference between $\Omega_{\text{within-crown}}$ and $\Omega_{\text{footprint}}$ indicates that the error of LAI acquired from directly applying Beer's law at the individual-tree level is smaller than that at the footprint/pixel level. The reason is that the between-crown gaps lead to an

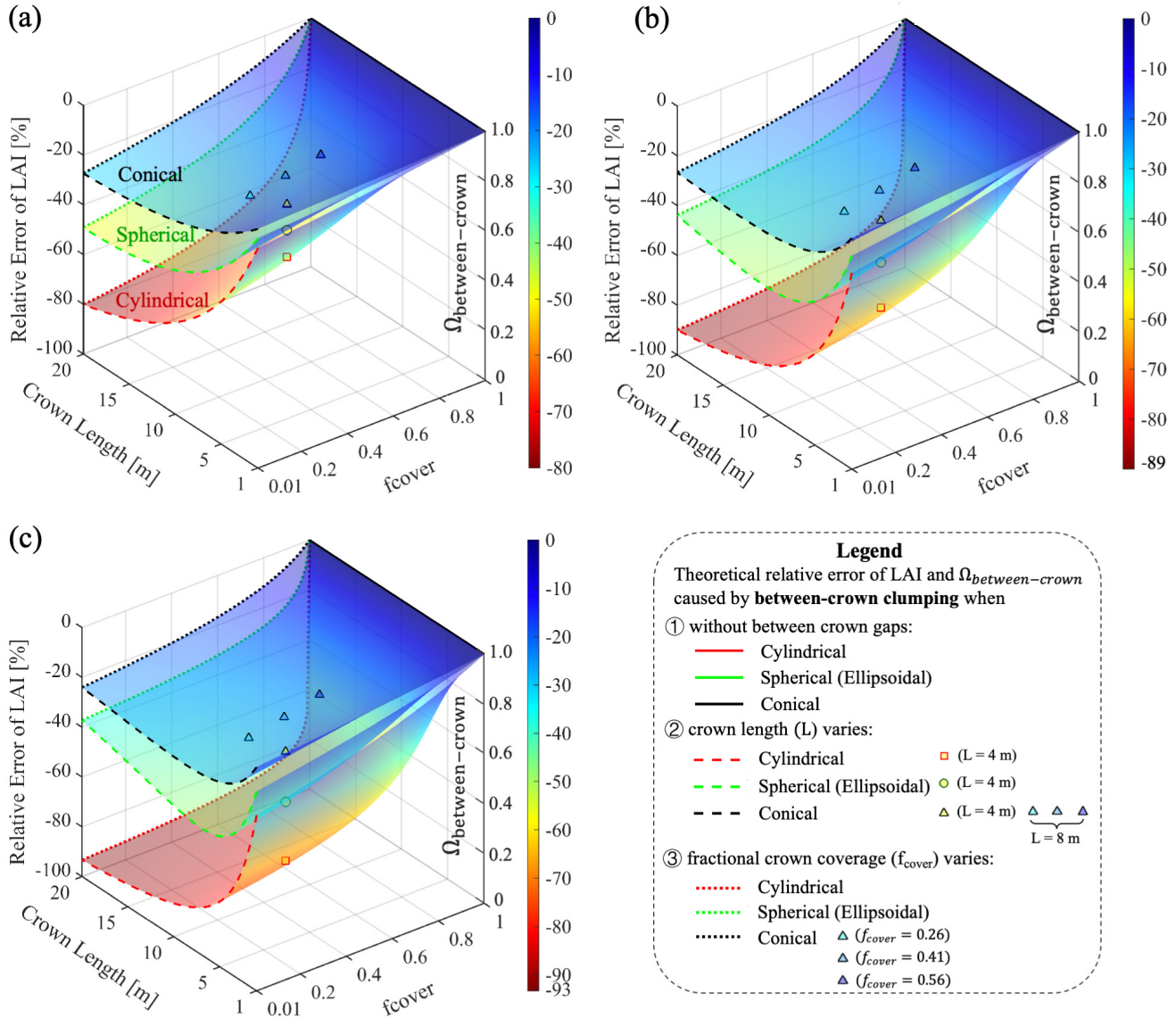


Fig. 8. Theoretical error in LAI underestimation and clumping index ($\Omega_{\text{between-crown}}$) caused by between-crown clumping for cylindrical, spherical (or ellipsoidal), and conical canopies, taking the crown length (1–20 m), fractional crown coverage (f_{cover}) (0.01–1), and leaf area density (ρ , unit: m^2/m^3) [(a) 0.5, (b) 1.0, and (c) 1.5] into consideration.

increase in heterogeneity, i.e., the scale effect when applying a nonlinear Beer's law in LAI retrieval is more severe [60].

Our result shows that the clumping effect is large for long crowns, consistent with what Kuusk *et al.* [61] found from ALS data of forest stands but is not consistent with other findings in ground-based LAI measurement using LAI-2000 [26]. The reason is that the view angles of the LAI-2000 instrument can see more crowns for taller canopies, which causes the foliage to appear almost randomly distributed [26]. However, the longer the crown, the more significant the heterogeneity in the nadir-observing direction for airborne or spaceborne laser scanning.

$\Omega_{\text{footprint}}$ estimated from 11 290 footprints ranges from 0.16 to 0.99 ($\mu = 0.78$, $\sigma = 0.15$), and the histogram is shown in Fig. 13.

Previous studies in ground-based LAI measurement show that indirect methods based on Beer's law might cause a 30%–70% underestimation of LAI because of nonrandom foliage distribution [22]–[24]. Inspired by the result in Figs. 11 and 13, we believe that the underestimation of LAI from spaceborne LiDAR could be highly variable, and the error of LAI_e increases as both the crown ρ and crown length increase. For instance, it could be up to 93% for discrete cylindrical canopy [Fig. 11(c)], and an up to 84% underestimation was found in the real forest. Note that the findings here apply to spaceborne LiDAR and can be used to understand the errors in pixel-level (including multiple tree crowns, such as 10-m grid in [62]) LAI_e retrieval using point clouds from small-footprint airborne LiDAR if the scan angle is close to nadir. For instance, for small scan angles,

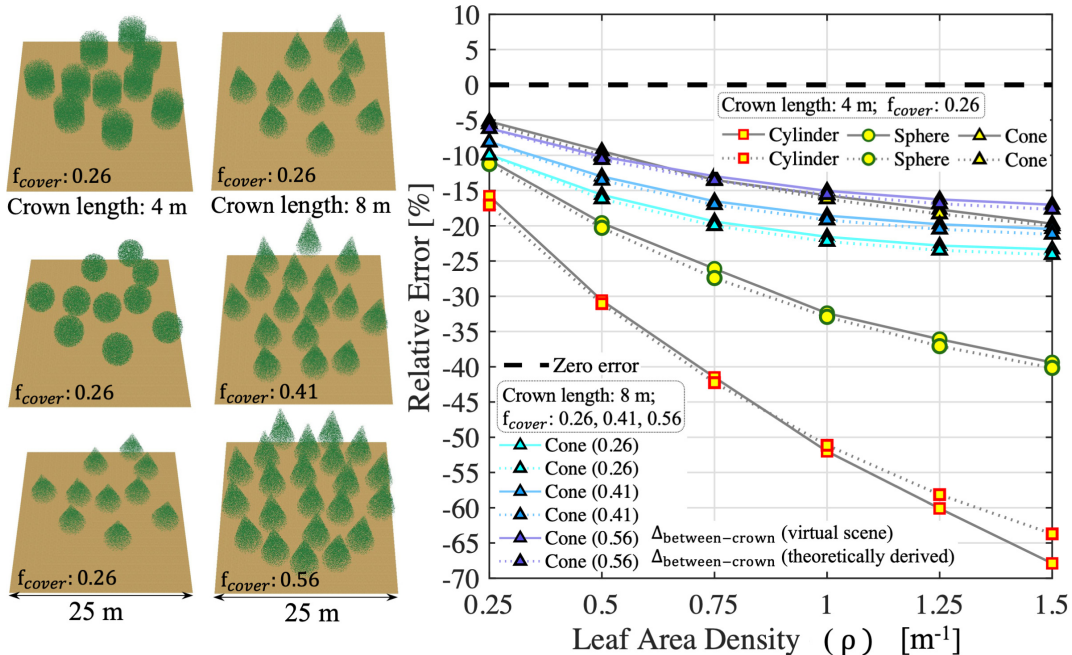


Fig. 9. Generated geometrical scenes (leaf area density (ρ , unit: m^2/m^3) = 0.75) and the relative errors of LAI (theoretically derived and those of the virtual scenes) caused by between-crown clumping from directly applying Beer's law, for discontinuous cylindrical, spherical, and conical canopies with the crown ρ ranging from 0.25 to 1.50, and the fractional crown coverage (f_{cover}) ranging from 0.26 to 0.56 with an increment of 0.15 for conical canopy: from the theoretical derivation (dotted lines) and the virtual scenes (solid lines).

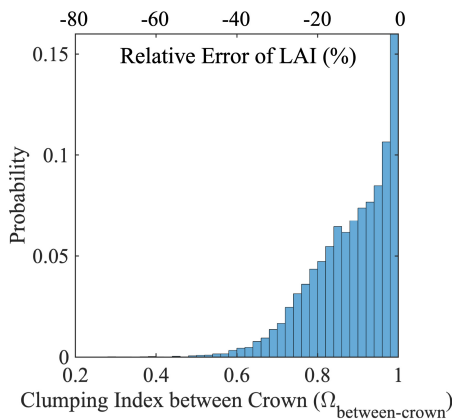


Fig. 10. Histogram of the between-crown clumping index ($\Omega_{\text{between-crown}}$) estimated from ALS point clouds data in 11 290 footprints with a diameter of 25 m.

no significant impact on proxies for fractional cover and LAI were observed in [63]. In addition, it was suggested that large off-nadir scan angle of small-footprint airborne LiDAR should be avoided to ensure a more accurate gap probability and LAI estimation in [57].

D. Dominant Contributing Factor in LAI Underestimation

Between-crown clumping and within-crown clumping are the main factors affecting the clumping effect. So far, there has been little attention on which one has greater impact on LAI underestimation. We calculated the difference between $|\Delta_{\text{within-crown}}|$ and $|\Delta_{\text{between-crown}}|$ to identify

the dominant factor from the theoretical derivation. For the real-world data $\Omega_{\text{within-crown}} < \Omega_{\text{between-crown}}$ indicates that the within-crown clumping is the dominant factor and vice versa.

The dominant clumping effect depends on the forest structure. 1) $\Delta_{\text{between-crown}}$ is the only contributing factor for the clumping effect in cylindrical canopies [Fig. 14(a1)–(a3)], which is highly variable from 0% (closed canopy) to 93% (very sparse canopy) at the long crown (20 m), large ρ (1.5), and small f_{cover} (0.01). In addition, the larger the crown ρ , the larger the required f_{cover} and the smaller the length of crown needed, to make the $|\Delta_{\text{between-crown}}|$ small enough to be neglected in LAI retrieval. 2) $\Delta_{\text{within-crown}}$ is roughly the dominant factor in the underestimation of LAI for discontinuous conical canopy [Fig. 14(c1)–(c3)]. However, 3) it depends on ρ , crown length, and f_{cover} for discontinuous spherical (ellipsoidal) canopy [Fig. 14(b1)–(b3)], and $\Delta_{\text{within-crown}}$ is the dominant contributing factor when f_{cover} is close to and over 0.9.

Identifying the dominant factor is of great significance for method development. It indicates that the method that corrects the between-crown clumping [21] (i.e., $\text{LAI}_{e_{f_{\text{cover}}}}$) makes a significant advancement in improving the LAI retrieval for cylindrical canopies from spaceborne LiDAR, where there is no within-crown clumping, while the between-crown clumping is the largest in all these three kinds of canopy. On the contrary, within-crown clumping is the dominant factor for conical canopies. In contrast, spherical canopies show a very complex situation that the dominant factor may change with f_{cover} , crown length, and ρ .

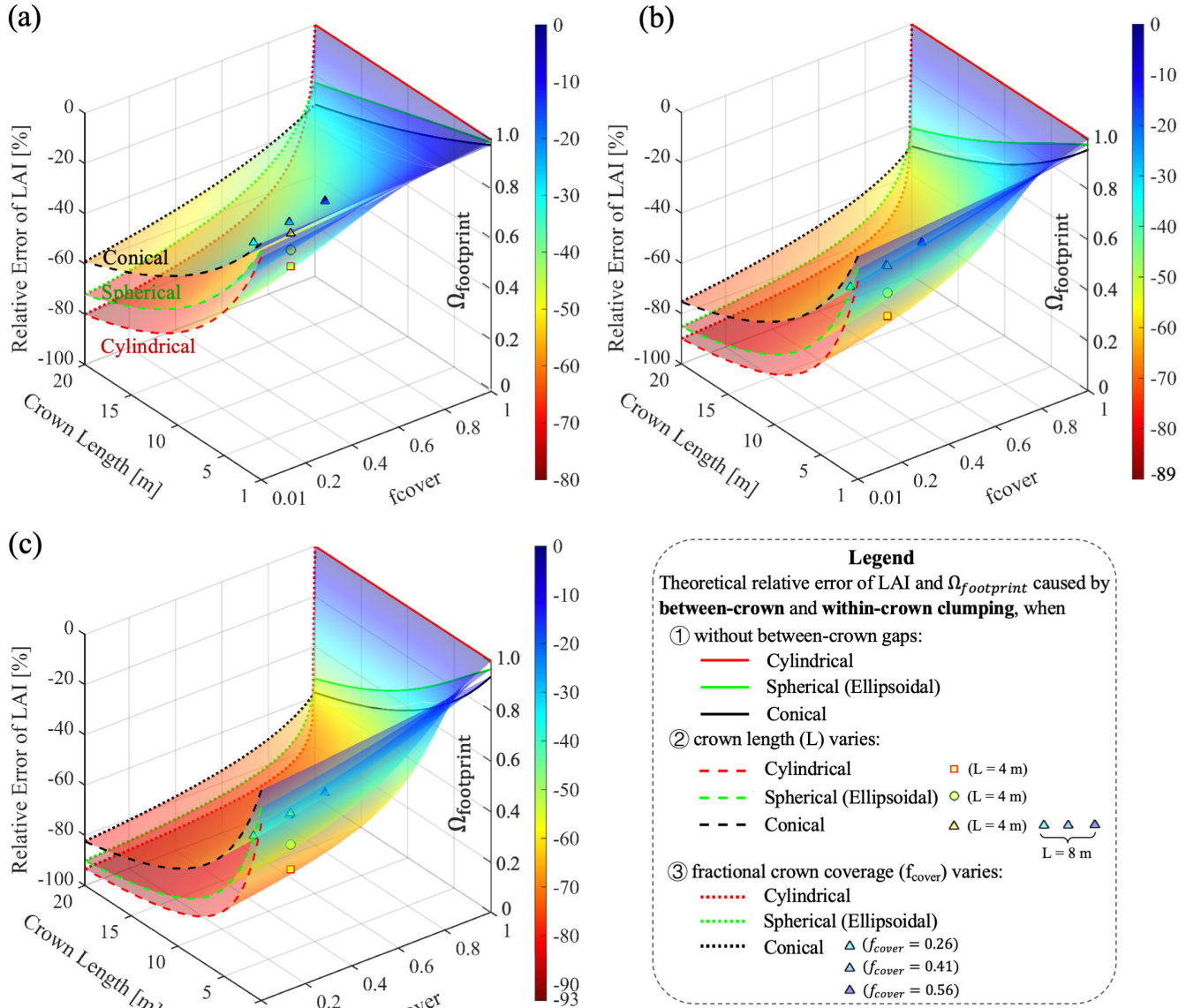


Fig. 11. Theoretical error in LAI underestimation and the total clumping index ($\Omega_{footprint}$) caused by the total clumping effect for cylindrical, spherical (or ellipsoidal), and conical canopies, taking the crown length (1–20 m), fractional crown coverage (f_{cover}) (0.01–1), and leaf area density (ρ , unit: m^2/m^3) [(a) 0.5, (b) 1.0, and (c) 1.5] into consideration.

In 47.4% of the footprints in real forests, within-crown clumping is the dominant contributing factor. The average $\Omega_{between-crown}$ and $\Omega_{within-crown}$ in each interval (with an increment of 0.1) of the value of $\Omega_{footprint}$ are shown in Fig. 15 (see Appendix for more details about the computed three kinds of clumping index, and the three kinds of LAI from not correcting any clumping to correcting both the between-crown clumping and within-crown clumping). It is noted that sometimes the within-crown clumping and the between-crown clumping dominate in different situations of the total clumping effect. This phenomenon is consistent with our theoretical derivation since the dominant factor depends on many factors, including the crown shape, crown length, f_{cover} , and the leaf area density.

E. Clumping Effects in Sloped Terrain

Both the within-crown clumping and between-crown clumping are not affected by topography. For within-crown clumping, Fig. 16 shows that path lengths (solid red lines in Fig. 16) that the rays pass through the trees on a sloped terrain [Fig. 16(a)] are the same as those on flat terrain [Fig. 16(b)]. It is because the observing direction of spaceborne LiDAR is close to nadir. However, when the observing direction deviates by a large amount from nadir, such as for TLS in Fig. 16, the path lengths (solid blue lines) are quite different from those on flat terrain, indicating that the within-crown clumping is influenced by topography. As shown in a previous study, topographic effects can lead to an

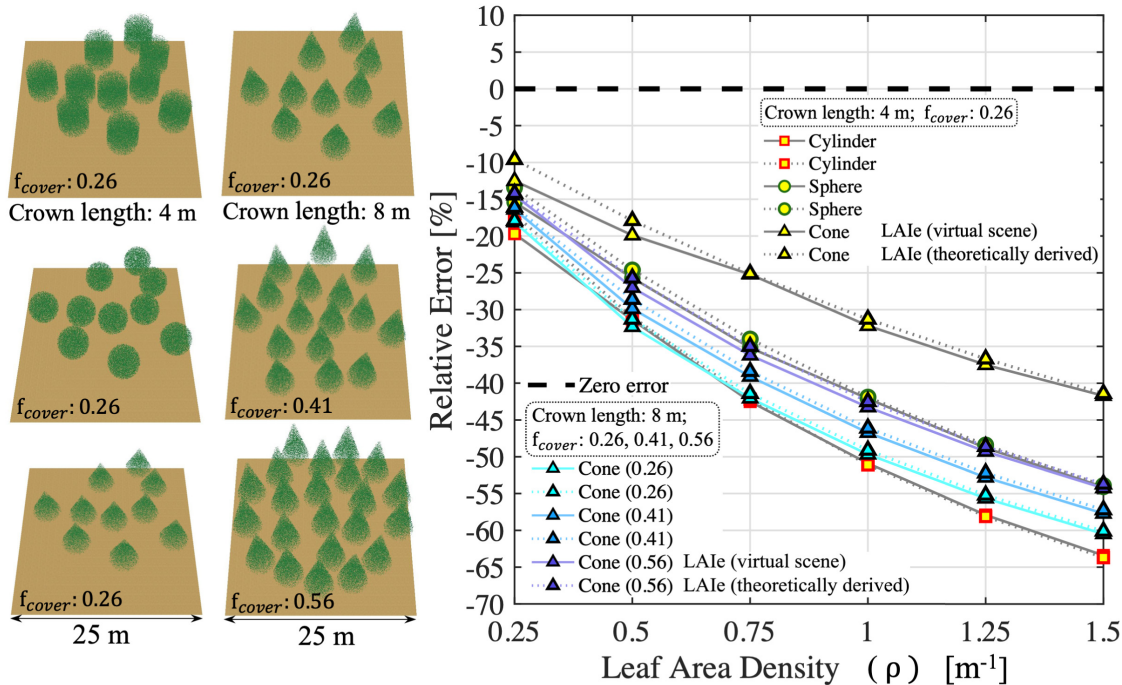


Fig. 12. Geometrical scenes (leaf area density (ρ , unit: m^2/m^3) = 0.75) and the relative errors of LAI caused by between-crown clumping and within-crown clumping together from directly applying Beer's law (LAI_e), for discontinuous cylindrical, spherical, and conical canopies with the crown ρ ranging from 0.25 to 1.50, and the fractional crown coverage (f_{cover}) ranging from 0.26 to 0.56 with an increment of 0.15 for conical canopy: from theoretical derivation (dotted lines) and the virtual scenes (solid lines).

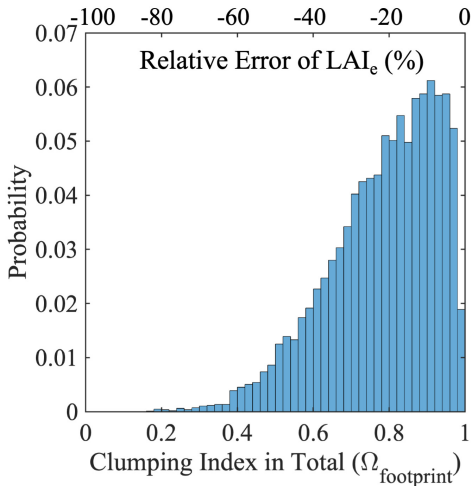


Fig. 13. Histogram of the total clumping index ($\Omega_{footprint}$) estimated from ALS point clouds data in 11 290 footprints with a diameter of 25 m. LAI_e denotes the effective LAI by assuming homogeneous vegetation in the footprint.

root mean square error (RMSE) up to 66.2% in the vertical distribution of the plant area [64]. For the between-crown clumping, the fraction of between-crown gaps (represented by brown lines in Fig. 16) is not affected by the topography. The between-crown gap probability is a fraction of between-crown gaps on the projected flat ground, not on a sloped terrain surface; in addition, the footprint size is defined by projection on flat ground as well.

The impact of the terrain on LAI retrieval is on the accuracy of the gap probability estimated from the waveform. Waveforms are stretched by the topography, leading to a mixing of return signals of vegetation and ground. This effect increases with terrain slope and undulation [65]. Moreover, previous studies [65], [66] show that it also manifests with footprint size (see Fig. 6 in [65] and Fig. 5 in [66])—comparisons of waveforms between footprint size of 25 and 70 m at different terrain slopes).

F. Research Perspectives

This study focuses on the influence of the clumping effect. The leaf projection coefficient (G), an essential parameter in Beer's law, is assumed to be 0.5 by assuming the leaf angle distribution to be spherical distribution. Real canopies might deviate from spherical distribution [67], [49], and it has been reported that this assumption might lead to an up to 53% underestimation of LAI_e when the viewing zenith angle is 0° [68]. The comprehensive influence of the clumping effect and the assumption of $G = 0.5$ on true LAI retrieval should be further studied. The unmanned aerial vehicle (UAV) laser scanning (UAVLS) system [69] has greater flexibility in scanning and can acquire higher point density when compared with ALS. It is promising in this topic because an *in situ* measurement of leaf angle distribution and LAI might be realized. For the leaf angle distribution estimation, the advantage of UAVLS in performing a hemispherical scanning, current issues, and perspectives has been discussed in [50, Sec. 4.4]. In contrast, Kuusk pointed that grouping together G and clumping index would be more rational [70]. Both G

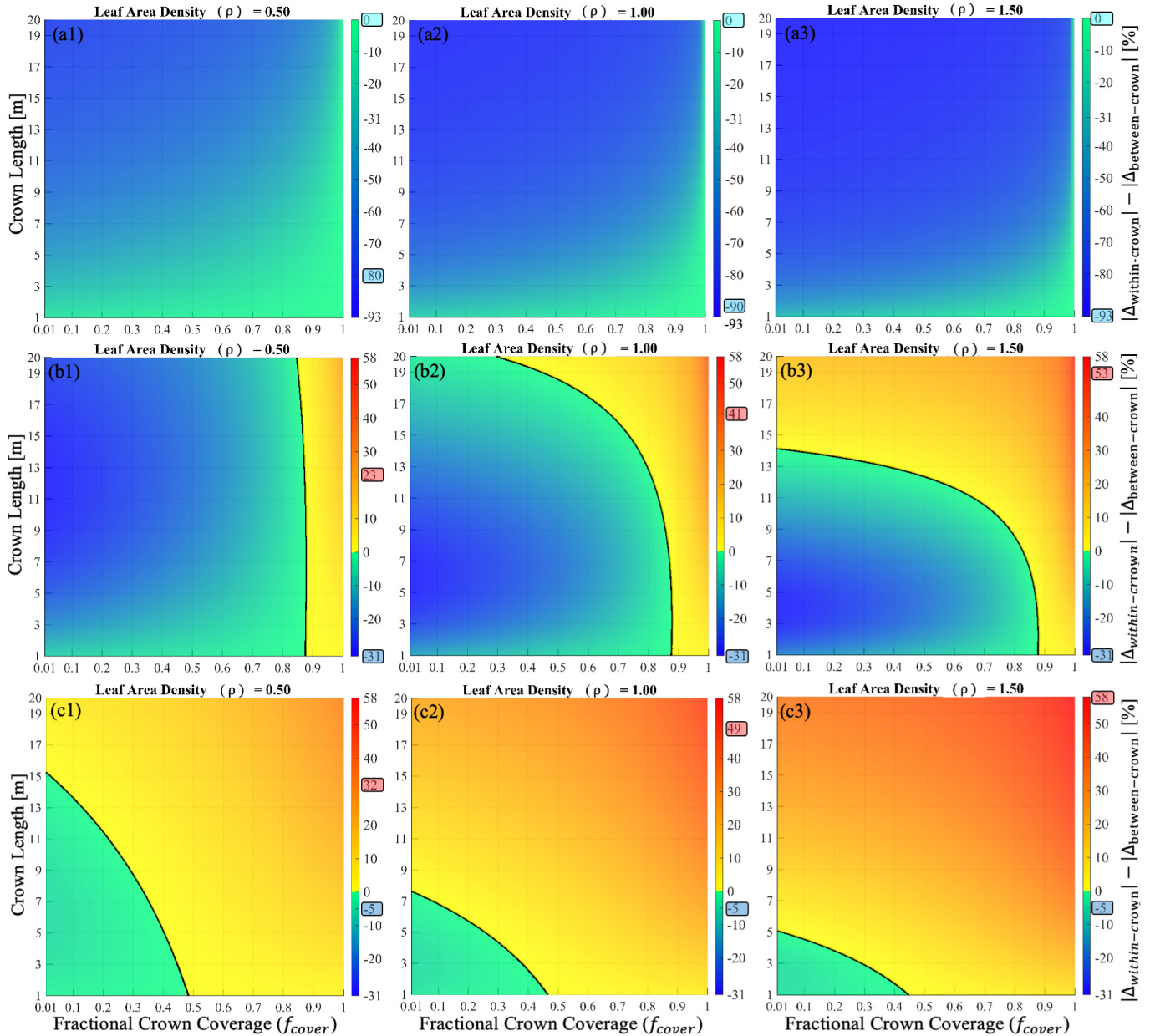


Fig. 14. Theoretical difference between the error caused by within-crown clumping ($|\Delta_{\text{within-crown}}|$) and between-crown clumping ($|\Delta_{\text{between-crown}}|$) for (a1)–(a3) cylindrical, (b1)–(b3) spherical (ellipsoidal), and (c1)–(c3) conical canopy in different conditions ($0.01 \leq f_{\text{cover}} \leq 1$, $1 \leq \text{crown length} \leq 20$) with the leaf area density (ρ , unit: m^2/m^3) set to be 0.5, 1.0, and 1.5, respectively. A negative value (on the left side of the black curve) and positive value (on the right side of the black curve) in (b1)–(b3) and (c1)–(c3) denotes that the between-crown clumping or within-crown clumping is the dominant factor in the underestimation of LAI.

and the clumping index are direction-dependent; whether this idea could provide more possibilities in LAI retrieval deserves further considerations, in theory.

Although the current spaceborne full-waveform LiDAR instruments show significant advantages in LAI retrieval due to its direct sampling of the 3-D vegetation structure, using the LiDAR data itself is not enough to ensure LAI retrieval accuracy because we cannot obtain the horizontal distribution information of the trees from such data. What can be estimated from the waveform is the total gap probability, which is a mixture of the between-crown and within-crown gap probability. However, separating them is crucial to correct either the

between-crown or the within-crown clumping. It is exactly why passive optical Landsat Thematic Mapper imagery was introduced to obtain the between-crown gaps for correcting the between-crown clumping in LAI retrieval from GLAS data in [21]. As one of the current physically based methods to retrieve LAI from spaceborne LiDAR, this method is superior in principle to the other method that directly applies Beer's law in the footprint. However, the differences in the viewing zenith angle, the geolocation accuracy, and the spatial resolution between different sensors on different platforms would inevitably introduce errors, limiting the application of this idea of joint use of the multisource data. In comparison,

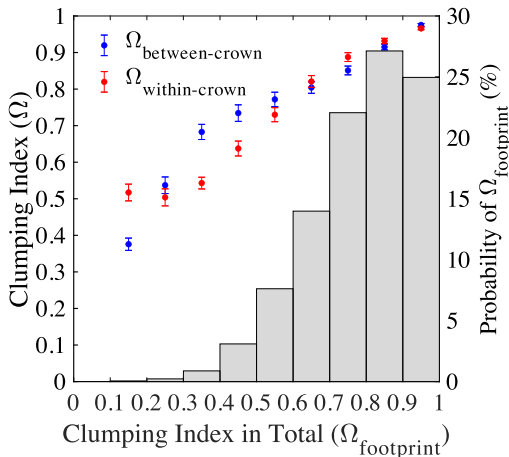


Fig. 15. Average between-crown ($\Omega_{\text{between-crown}}$) and within-crown clumping ($\Omega_{\text{within-crown}}$) indices (95% confidence interval) in each interval (with an increment of 0.1) of the total clumping index ($\Omega_{\text{footprint}}$). The right axis shows the percentage of the footprints ($N = 11\,290$) with the value of $\Omega_{\text{footprint}}$ in a specific interval in all the footprints with a diameter of 25 m. $\Omega_{\text{within-crown}} < \Omega_{\text{between-crown}}$ indicates that the within-crown clumping is the dominant contributing factor in LAI retrieval.

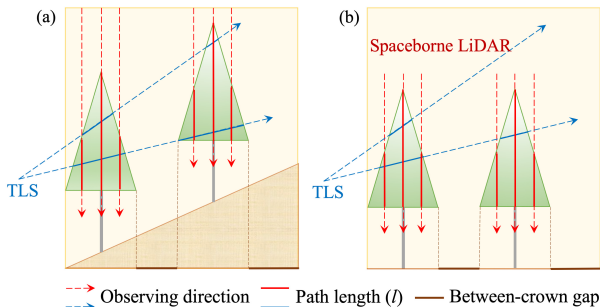


Fig. 16. Path lengths that the rays pass through the trees on (a) sloped and (b) flat terrain, and the between-crown gaps. TLS denotes terrestrial laser scanning.

the method of directly applying Beer's law has been widely used due to its advantages in applicability and simplicity.

The future improvement of the LAI retrieval from the spaceborne LiDAR could focus on two aspects: instrument design and method research. From the perspective of instrument design, a simultaneous measurement of a laser scanner and high-resolution imagery on the same platform would be promising in improving LAI retrieval, especially for the nonnegligible between-crown clumping in sparse forests (see Fig. 8). The upcoming MOLI [12], which will conduct a simultaneous measurement using a laser scanner (25-m diameter footprint) and an imager (green, red, and near-infrared band, with 5-m spatial resolution), would be a good data source. However, what the spatial resolution of the imagery should be to make sure that the fractional crown coverage information can be acquired accurately still needs further investigation. Simulating the passive optical imagery (with different spatial resolutions) and the waveform through a 3-D radiative transfer model such as DART [71] would be a pathway to provide data. From the perspective of method research, fully utilizing the 3-D sampling information in the waveform to correct the within-crown clumping, instead of only using the 2-D gap probability, would deserve further study.

This study contributes to understanding the mechanism of the clumping effect in between-crown, crown, and footprint levels. It provides some insights on improving LAI retrieval from large-footprint LiDAR and offers potential explanations for errors in pixel-level effective LAI retrieval from ALS point clouds data when scan angles close to nadir are used. In addition, the clumping effects in various forest structures are helpful for better understanding the modeling of the directional gap probability and the hotspot effect [72], which are affected by the between-crown clumping and within-crown clumping, in the radiative transfer model [73].

VI. CONCLUSION

Most physically based methods of LAI retrieval from large-footprint LiDAR are based on Beer's law, assuming random foliage spatial distribution in the entire footprint. Some studies have corrected for the between-crown clumping, but still assume randomness in crown-covered regions. As a result, there is usually an underestimation of LAI due to the heterogeneity of the forest canopy. This study quantitatively investigated the between-crown, the within-crown, and the total clumping effect at a large-footprint LiDAR scale both through a theoretical derivation and by using ALS point clouds data in Aargau, Switzerland. Based on the definition of the clumping index, we theoretically analyzed the clumping effects with various forest structure parameters including different crown shapes, crown lengths, crown leaf area densities, and fractional crown coverages in the footprint, making the causes of the clumping effect clear.

The computed clumping indices from the theoretical derivation and ALS data in 11 290 footprints (diameter = 25 m) indicate the nonnegligible clumping effect from the spaceborne LiDAR perspective. The range of the total clumping index is found to be 0.07–1.0 from theoretical derivation and 0.16–1.0 from real-world data. It increases with crown length and crown leaf area density but decreases with increasing fractional crown coverage, and is larger than that at the individual tree level. Correcting for between-crown clumping ($\Omega_{\text{between-crown}}$ ranges from 0.29 to 1.0 in real-world data) improves LAI retrieval significantly; however, the error caused by within-crown clumping ($\Omega_{\text{within-crown}}$ ranges from 0.31 to 1.0 in real-world data), which increases with crown length and crown leaf area density, and is larger for conical than that for spherical (ellipsoidal) canopies, cannot be neglected. We found that.

- 1) When there are between-crown gaps, conical canopies with short crowns, small crown leaf area densities, and high fractional crown coverages are associated with the lowest error in LAI retrieval by directly using Beer's law.
- 2) Cylindrical canopies are suitable for using the method which just corrects between-crown clumping.
- 3) The error could be up to 93% caused by between-crown clumping for cylindrical canopies and up to 58% caused by within-crown clumping for conical canopies, and the corresponding errors caused by between-crown clumping and within-crown clumping for spherical canopies

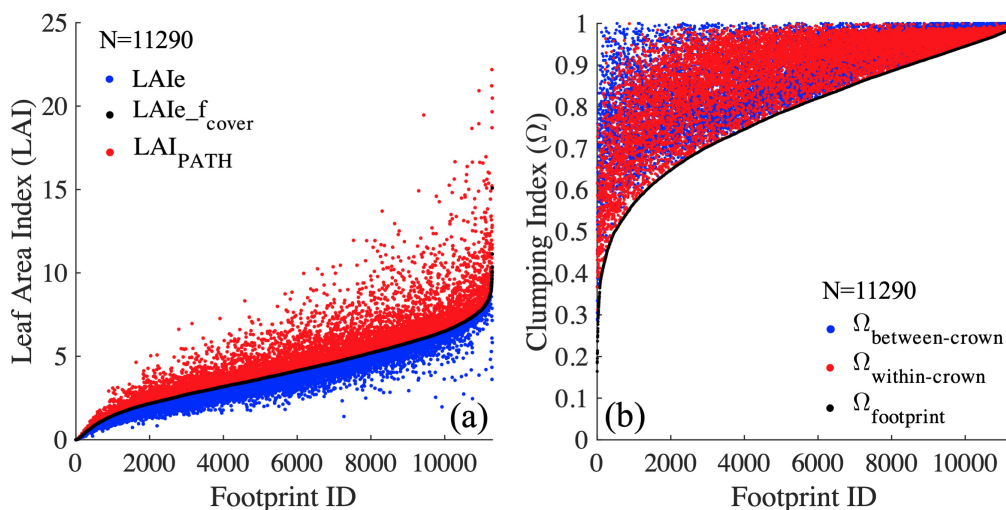


Fig. 17. (a) Scatter plot of three LAIs (LAI_e —using homogeneity assumption, $LAI_{e_f_cover}$ —correcting the between-crown clumping, and LAI_{PATH} —correcting both the between-crown clumping and within-crown clumping) and (b) between-crown, within-crown, and total clumping indices.

are smaller than these two values, respectively. Correspondingly, the dominant factor in the underestimation of LAI is related to the canopy types: it is between-crown clumping for cylindrical canopies and within-crown clumping for conical canopies, while it depends on the specific fractional crown coverage, crown length, and leaf area density for spherical canopies.

Correcting for between-crown clumping is an important contribution to the improvement of LAI retrieval accuracy, and our results highlight the importance of further correction of the clumping effect in the crown-covered regions to improve LAI retrieval in the future.

APPENDIX

LAI_s [Fig. 17(a)] from not correcting any clumping to correcting both the between-crown clumping and within-crown clumping, and the clumping indices [Fig. 17(b)] at the between-crown, crown, and footprint scale were computed from the ALS point clouds data in 11 290 footprints with a diameter of 25 m. We sorted all the results in ascending order according to $LAI_{e_f_cover}$ and the total clumping index ($\Omega_{footprint}$) to show the differences of the three LAIs [Fig. 17(a)] and the three clumping indices [Fig. 17(b)], respectively.

ACKNOWLEDGMENT

The authors gratefully acknowledge the three anonymous reviewers for their thoughtful and constructive reviews that helped significantly improve the quality of this article.

REFERENCES

- [1] J. M. Chen and T. A. Black, "Defining leaf area index for non-flat leaves," *Plant, Cell Environ.*, vol. 15, no. 4, pp. 421–429, May 1992, doi: [10.1111/j.1365-3040.1992.tb00992.x](https://doi.org/10.1111/j.1365-3040.1992.tb00992.x).
- [2] G. Yan *et al.*, "Review of indirect optical measurements of leaf area index: Recent advances, challenges, and perspectives," *Agricult. Forest Meteorol.*, vol. 265, pp. 390–411, Feb. 2019.
- [3] G. P. Asner, J. M. O. Scurlock, and J. A. Hicke, "Global synthesis of leaf area index observations: Implications for ecological and remote sensing studies," *Global Ecol. Biogeogr.*, vol. 12, pp. 191–205, May 2003, doi: [10.1046/j.1466-822X.2003.00026.x](https://doi.org/10.1046/j.1466-822X.2003.00026.x).
- [4] J. Tian, L. Wang, and X. Li, "Sub-footprint analysis to uncover tree height variation using ICESat/GLAS," *Int. J. Appl. Earth Observ. Geoinf.*, vol. 35, pp. 284–293, Mar. 2015, doi: [10.1016/j.jag.2014.09.016](https://doi.org/10.1016/j.jag.2014.09.016).
- [5] S. C. Stark *et al.*, "Amazon forest carbon dynamics predicted by profiles of canopy leaf area and light environment," *Ecol. Lett.*, vol. 15, no. 12, pp. 1406–1414, Dec. 2012, doi: [10.1111/j.1461-0248.2012.01864.x](https://doi.org/10.1111/j.1461-0248.2012.01864.x).
- [6] J. B. Drake *et al.*, "Estimation of tropical forest structural characteristics, using large-footprint LiDAR," *Remote Sens. Environ.*, vol. 79, nos. 2–3, pp. 305–319, 2002, doi: [10.1016/S0034-4257\(01\)00281-4](https://doi.org/10.1016/S0034-4257(01)00281-4).
- [7] M. A. Lefsky, W. B. Cohen, G. G. Parker, and D. J. Harding, "LiDAR remote sensing for ecosystem studies," *Bioscience*, vol. 52, no. 1, pp. 19–30, 2002, doi: [10.1641/0006-3568\(2002\)052\[0019:LRSFES\]2.0.CO;2](https://doi.org/10.1641/0006-3568(2002)052[0019:LRSFES]2.0.CO;2).
- [8] S. Hancock *et al.*, "Waveform LiDAR over vegetation: An evaluation of inversion methods for estimating return energy," *Remote Sens. Environ.*, vol. 164, pp. 208–224, Jul. 2015, doi: [10.1016/j.rse.2015.04.013](https://doi.org/10.1016/j.rse.2015.04.013).
- [9] W. Ni-Meister, D. L. B. Jupp, and R. Dubayah, "Modeling LiDAR waveforms in heterogeneous and discrete canopies," *IEEE Trans. Geosci. Remote Sens.*, vol. 39, no. 9, pp. 1943–1958, Sep. 2001, doi: [10.1109/36.951085](https://doi.org/10.1109/36.951085).
- [10] R. S. Afzal *et al.*, "The geoscience laser altimeter system (GLAS) laser transmitter," *IEEE J. Sel. Topics Quantum Electron.*, vol. 13, no. 3, pp. 511–535, May/June 2007, doi: [10.1109/JSTQE.2007.896051](https://doi.org/10.1109/JSTQE.2007.896051).
- [11] R. Dubayah *et al.*, "The global ecosystem dynamics investigation: High-resolution laser ranging of the Earth's forests and topography," *Sci. Remote Sens.*, vol. 1, Jun. 2020, Art. no. 100002, doi: [10.1016/j.srs.2020.100002](https://doi.org/10.1016/j.srs.2020.100002).
- [12] D. Sakaizawa, R. Mitsuhahi, J. Murooka, T. Imai, T. Kimura, and K. Asai, "Current status of the ISS-vegetation LiDAR mission-MOLI," in *Proc. Int. Geosci. Remote Sens. Symp. (IGARSS)*, 2018, pp. 1861–1864, doi: [10.1109/IGARSS.2018.8518379](https://doi.org/10.1109/IGARSS.2018.8518379).
- [13] W. Yang *et al.*, "MODIS leaf area index products: From validation to algorithm improvement," *IEEE Trans. Geosci. Remote Sens.*, vol. 44, no. 7, pp. 1885–1896, Jul. 2006, doi: [10.1109/TGRS.2006.871215](https://doi.org/10.1109/TGRS.2006.871215).
- [14] X. Li and A. H. Strahler, "Geometric-optical bidirectional reflectance modeling of a conifer forest canopy," *IEEE Trans. Geosci. Remote Sens.*, vol. GE-24, no. 6, pp. 906–919, Nov. 1986, doi: [10.1109/TGRS.1986.289706](https://doi.org/10.1109/TGRS.1986.289706).
- [15] J. M. Chen and S. G. Leblanc, "A four-scale bidirectional reflectance model based on canopy architecture," *IEEE Trans. Geosci. Remote Sens.*, vol. 35, no. 5, pp. 1316–1337, Sep. 1997, doi: [10.1109/36.628798](https://doi.org/10.1109/36.628798).
- [16] A. Beer, "Bestimmung der absorption des rothen lichts in farbigen flüssigkeiten," *Annalen Physik Chem.*, vol. 162, no. 5, pp. 78–88, 1852, doi: [10.1002/andp.18521620505](https://doi.org/10.1002/andp.18521620505).

- [17] T. Nilson, "A theoretical analysis of the frequency of gaps in plant stands," *Agricult. Meteorol.*, vol. 8, pp. 25–38, Jan. 1971, doi: [10.1016/0002-1571\(71\)90092-6](https://doi.org/10.1016/0002-1571(71)90092-6).
- [18] T. Nilson, "Inversion of gap frequency data in forest stands," *Agricult. Forest Meteorol.*, vols. 98–99, pp. 437–448, Dec. 1999, doi: [10.1016/S0168-1923\(99\)00114-8](https://doi.org/10.1016/S0168-1923(99)00114-8).
- [19] J. L. Monteith, "Light distribution and photosynthesis in field crops," *Ann. Botany*, vol. 29, no. 1, pp. 17–37, Jan. 1965, doi: [10.1093/oxfordjournals.aob.a083934](https://doi.org/10.1093/oxfordjournals.aob.a083934).
- [20] C. T. De Wit, "Photosynthesis of leaf canopies. Agri-cultural Research Report No 663," in *Center for Agri-Cultural Publication and Documentation*. Wageningen, The Netherlands, 1965, pp. 1–57.
- [21] X. Yang, C. Wang, F. Pan, S. Nie, X. Xi, and S. Luo, "Retrieving leaf area index in discontinuous forest using ICESat/GLAS full-waveform data based on gap fraction model," *ISPRS J. Photogramm. Remote Sens.*, vol. 148, pp. 54–62, Feb. 2019, doi: [10.1016/j.isprsjprs.2018.12.010](https://doi.org/10.1016/j.isprsjprs.2018.12.010).
- [22] J. M. Chen and J. Cihlar, "Quantifying the effect of canopy architecture on optical measurements of leaf area index using two gap size analysis methods," *IEEE Trans. Geosci. Remote Sens.*, vol. 33, no. 3, pp. 777–787, May 1995, doi: [10.1109/36.387593](https://doi.org/10.1109/36.387593).
- [23] P. Stenberg, "Correcting LAI-2000 estimates for the clumping of needles in shoots of conifers," *Agric. Forest Meteorol.*, vol. 79, nos. 1–2, pp. 1–8, Mar. 1996, doi: [10.1016/0168-1923\(95\)02274-0](https://doi.org/10.1016/0168-1923(95)02274-0).
- [24] M. Weiss, F. Baret, G. J. Smith, I. Jonckheere, and P. Coppin, "Review of methods for *in situ* leaf area index (LAI) determination," *Agricult. Forest Meteorol.*, vol. 121, nos. 1–2, pp. 37–53, Jan. 2004, doi: [10.1016/j.agrformet.2003.08.001](https://doi.org/10.1016/j.agrformet.2003.08.001).
- [25] X. Zhu *et al.*, "Improving leaf area index (LAI) estimation by correcting for clumping and woody effects using terrestrial laser scanning," *Agricult. Forest Meteorol.*, vol. 263, pp. 276–286, Dec. 2018, doi: [10.1016/j.agrformet.2018.08.026](https://doi.org/10.1016/j.agrformet.2018.08.026).
- [26] Y. Ryu, T. Nilson, H. Kobayashi, O. Sonnentag, B. E. Law, and D. D. Baldocchi, "On the correct estimation of effective leaf area index: Does it reveal information on clumping effects?" *Agricult. Forest Meteorol.*, vol. 150, no. 3, pp. 463–472, Mar. 2010, doi: [10.1016/j.agrformet.2010.01.009](https://doi.org/10.1016/j.agrformet.2010.01.009).
- [27] L. Ma, G. Zheng, X. Wang, S. Li, Y. Lin, and W. Ju, "Retrieving forest canopy clumping index using terrestrial laser scanning data," *Remote Sens. Environ.*, vol. 210, pp. 452–472, Jun. 2018, doi: [10.1016/j.rse.2018.03.034](https://doi.org/10.1016/j.rse.2018.03.034).
- [28] J. M. Chen, C. H. Menges, and S. G. Leblanc, "Global mapping of foliage clumping index using multi-angular satellite data," *Remote Sens. Environ.*, vol. 97, pp. 447–457, Sep. 2005, doi: [10.1016/j.rse.2005.05.003](https://doi.org/10.1016/j.rse.2005.05.003).
- [29] A. Brenner *et al.*, "Derivation of range and range distributions from laser pulse waveform analysis for surface elevations, roughness, slope, and vegetation heights, algorithm theoretical basis document, v.4.1," Tech. Rep., 2003. [Online]. Available: http://www.csr.utexas.edu/glas/pdf/Atbd_20031224.pdf
- [30] H. Tang and J. Armston, "Algorithm theoretical basis document (ATBD) for GEDI L2B footprint canopy cover and vertical profile metrics," Goddard Space Flight Center, Greenbelt, MD, USA, Tech. Rep., 2019. [Online]. Available: https://lpdaac.usgs.gov/documents/588/GEDI_FCCVPM_ATBD_v1.0.pdf
- [31] H. Fang, Y. Ye, W. Liu, S. Wei, and L. Ma, "Continuous estimation of canopy leaf area index (LAI) and clumping index over broadleaf crop fields: An investigation of the PASTIS-57 instrument and smartphone applications," *Agricult. Forest Meteorol.*, vols. 253–254, pp. 48–61, May 2018, doi: [10.1016/j.agrformet.2018.02.003](https://doi.org/10.1016/j.agrformet.2018.02.003).
- [32] C. J. Kucharik, J. M. Norman, L. M. Murdock, and S. T. Gower, "Characterizing canopy nonrandomness with a multiband vegetation imager (MVI)," *J. Geophys. Res.*, vol. 102, no. D24, pp. 29455–29473, Dec. 1997.
- [33] R. K. Braghieri *et al.*, "Influence of sun zenith angle on canopy clumping and the resulting impacts on photosynthesis," *Agricult. Forest Meteorol.*, vol. 291, Sep. 2020, Art. no. 108065, doi: [10.1016/j.agrformet.2020.108065](https://doi.org/10.1016/j.agrformet.2020.108065).
- [34] H. Fang, "Canopy clumping index (CI): A review of methods, characteristics, and applications," *Agricult. Forest Meteorol.*, vol. 303, Jun. 2021, Art. no. 108374, doi: [10.1016/j.agrformet.2021.108374](https://doi.org/10.1016/j.agrformet.2021.108374).
- [35] R. K. Braghieri *et al.*, "Accounting for canopy structure improves hyperspectral radiative transfer and sun-induced chlorophyll fluorescence representations in a new generation Earth system model" *Remote Sens. Environ.*, vol. 261, Aug. 2021, Art. no. 112497, doi: [10.1016/j.rse.2021.112497](https://doi.org/10.1016/j.rse.2021.112497).
- [36] Y. Ryu *et al.*, "How to quantify tree leaf area index in an open savanna ecosystem: A multi-instrument and multi-model approach," *Agricult. Forest Meteorol.*, vol. 150, no. 1, pp. 63–76, Jan. 2010, doi: [10.1016/j.agrformet.2009.08.007](https://doi.org/10.1016/j.agrformet.2009.08.007).
- [37] R. Hu, G. Yan, X. Mu, and J. Luo, "Indirect measurement of leaf area index on the basis of path length distribution," *Remote Sens. Environ.*, vol. 155, pp. 239–247, Dec. 2014, doi: [10.1016/j.rse.2014.08.032](https://doi.org/10.1016/j.rse.2014.08.032).
- [38] J. M. Chen, A. Govind, O. Sonnentag, Y. Zhang, A. Barr, and B. Amiro, "Leaf area index measurements at Fluxnet-Canada forest sites," *Agricult. Forest Meteorol.*, vol. 140, nos. 1–4, pp. 257–268, Nov. 2006, doi: [10.1016/j.agrformet.2006.08.005](https://doi.org/10.1016/j.agrformet.2006.08.005).
- [39] H. Tang *et al.*, "Deriving and validating Leaf Area Index (LAI) at multiple spatial scales through lidar remote sensing: A case study in Sierra National Forest, CA," *Remote Sens. Environ.*, vol. 143, pp. 131–141, Mar. 2014, doi: [10.1016/j.rse.2013.12.007](https://doi.org/10.1016/j.rse.2013.12.007).
- [40] H. Tang *et al.*, "Retrieval of vertical LAI profiles over tropical rain forests using waveform lidar at La Selva, Costa Rica," *Remote Sens. Environ.*, vol. 124, pp. 242–250, Sep. 2012, doi: [10.1016/j.rse.2012.05.005](https://doi.org/10.1016/j.rse.2012.05.005).
- [41] T. A. Black, J.-M. Chen, X. Lee, and R. M. Sagar, "Characteristics of shortwave and longwave irradiances under a Douglas-fir forest stand," *Can. J. Forest Res.*, vol. 21, no. 7, pp. 1020–1028, Jul. 1991, doi: [10.1139/x91-140](https://doi.org/10.1139/x91-140).
- [42] G. Sun and K. J. Ranson, "Modeling LiDAR returns from forest canopies," *IEEE Trans. Geosci. Remote Sens.*, vol. 38, no. 6, pp. 2617–2626, Nov. 2000, doi: [10.1109/36.885208](https://doi.org/10.1109/36.885208).
- [43] M. Béland, J.-L. Widlowski, R. A. Fournier, J.-F. Côté, and M. M. Verstraete, "Estimating leaf area distribution in savanna trees from terrestrial LiDAR measurements," *Agric. Forest Meteorol.*, vol. 151, no. 9, pp. 1252–1266, Sep. 2011, doi: [10.1016/j.agrformet.2011.05.004](https://doi.org/10.1016/j.agrformet.2011.05.004).
- [44] L. Cui *et al.*, "Retrieving forest canopy elements clumping index using ICESat GLAS LiDAR data," *Remote Sens.*, vol. 13, no. 5, p. 948, 2021, doi: [10.3390/rs13050948](https://doi.org/10.3390/rs13050948).
- [45] Y. Wang and H. Fang, "Estimation of LAI with the LiDAR technology: A review," *Remote Sens.*, vol. 12, no. 20, p. 3457, 2020, doi: [10.3390/rs12203457](https://doi.org/10.3390/rs12203457).
- [46] R. Hu *et al.*, "Using airborne laser scanner and path length distribution model to quantify clumping effect and estimate leaf area index," *IEEE Trans. Geosci. Remote Sens.*, vol. 56, no. 6, pp. 3196–3209, Jun. 2018, doi: [10.1109/TGRS.2018.2794504](https://doi.org/10.1109/TGRS.2018.2794504).
- [47] G. Wang, G. Gertner, S. Fang, and A. B. Anderson, "Mapping vegetation cover change using geostatistical methods and bitemporal Landsat TM images," *IEEE Trans. Geosci. Remote Sens.*, vol. 42, no. 3, pp. 632–643, Mar. 2004, doi: [10.1109/TGRS.2004.823450](https://doi.org/10.1109/TGRS.2004.823450).
- [48] G. Zheng and L. M. Moskal, "Leaf orientation retrieval from terrestrial laser scanning (TLS) data," *IEEE Trans. Geosci. Remote Sens.*, vol. 50, no. 10, pp. 3970–3979, Oct. 2012, doi: [10.1109/TGRS.2012.2188533](https://doi.org/10.1109/TGRS.2012.2188533).
- [49] J. Liu *et al.*, "Variation of leaf angle distribution quantified by terrestrial LiDAR in natural European beech forest," *ISPRS J. Photogramm. Remote Sens.*, vol. 148, pp. 208–220, Feb. 2019, doi: [10.1016/j.isprsjprs.2019.01.005](https://doi.org/10.1016/j.isprsjprs.2019.01.005).
- [50] H. Jiang *et al.*, "Influencing factors in estimation of leaf angle distribution of an individual tree from terrestrial laser scanning data," *Remote Sens.*, vol. 13, no. 6, p. 1159, Mar. 2021, doi: [10.3390/rs13061159](https://doi.org/10.3390/rs13061159).
- [51] J. P. Gastellu-Etchegorry, E. Martin, and F. Gascon, "DART: A 3D model for simulating satellite images and studying surface radiation budget," *Int. J. Remote Sens.*, vol. 25, pp. 73–96, Jan. 2004, doi: [10.1080/0143116031000115166](https://doi.org/10.1080/0143116031000115166).
- [52] M. Milenković, W. Wagner, R. Quast, M. Hollaus, C. Ressler, and N. Pfeifer, "Total canopy transmittance estimated from small-footprint, full-waveform airborne LiDAR," *ISPRS J. Photogramm. Remote Sens.*, vol. 128, pp. 61–72, Jun. 2017, doi: [10.1016/j.isprsjprs.2017.03.008](https://doi.org/10.1016/j.isprsjprs.2017.03.008).
- [53] T. Yin, J. Qi, B. D. Cook, D. C. Morton, S. Wei, and J.-P. Gastellu-Etchegorry, "Modeling small-footprint airborne LiDAR-derived estimates of gap probability and leaf area index," *Remote Sens.*, vol. 12, no. 1, p. 4, Dec. 2019, doi: [10.3390/RS12010004](https://doi.org/10.3390/RS12010004).
- [54] B. Bailey, M. P. de León, and E. S. Krayenhoff, "One-dimensional models of radiation transfer in heterogeneous canopies: A review, re-evaluation, and improved model," *Geosci. Model Develop.*, vol. 13, no. 10, pp. 4789–4808, 2020, doi: [10.5194/gmd-2019-305](https://doi.org/10.5194/gmd-2019-305).
- [55] G. Ligot, P. Balandier, B. Courbaud, and H. Claessens, "Forest radiative transfer models: Which approach for which application?" *Can. J. Forest Res.*, vol. 44, no. 5, pp. 391–403, May 2014, doi: [10.1139/cjfr-2013-0494](https://doi.org/10.1139/cjfr-2013-0494).
- [56] Y. Pang, M. Lefsky, G. Sun, and J. Ranson, "Impact of footprint diameter and off-nadir pointing on the precision of canopy height estimates from spaceborne LiDAR," *Remote Sens. Environ.*, vol. 115, no. 11, pp. 2798–2809, 2011, doi: [10.1016/j.rse.2010.08.025](https://doi.org/10.1016/j.rse.2010.08.025).
- [57] J. Liu *et al.*, "Large off-nadir scan angle of airborne LiDAR can severely affect the estimates of forest structure metrics," *ISPRS J. Photogramm. Remote Sens.*, vol. 136, pp. 13–25, Feb. 2018, doi: [10.1016/j.isprsjprs.2017.12.004](https://doi.org/10.1016/j.isprsjprs.2017.12.004).

- [58] C. J. Kucharik, J. M. Norman, and S. T. Gower, "Measurements of branch area and adjusting leaf area index indirect measurements," *Agric. Forest Meteorol.*, vol. 91, nos. 1–2, pp. 69–88, May 1998, doi: [10.1016/S0168-1923\(98\)00064-1](https://doi.org/10.1016/S0168-1923(98)00064-1).
- [59] S. G. Leblanc, J. M. Chen, R. Fernandes, D. W. Deering, and A. Conley, "Methodology comparison for canopy structure parameters extraction from digital hemispherical photography in boreal forests," *Agric. Forest Meteorol.*, vol. 129, nos. 3–4, pp. 187–207, Apr. 2005, doi: [10.1016/j.agrformet.2004.09.006](https://doi.org/10.1016/j.agrformet.2004.09.006).
- [60] G. Yan *et al.*, "Scale effect in indirect measurement of leaf area index," *IEEE Trans. Geosci. Remote Sens.*, vol. 54, no. 6, pp. 3475–3484, Jun. 2016, doi: [10.1109/TGRS.2016.2519098](https://doi.org/10.1109/TGRS.2016.2519098).
- [61] A. Kuusk, J. Pisek, M. Lang, and S. Mårdla, "Estimation of gap fraction and foliage clumping in forest canopies," *Remote Sens.*, vol. 10, no. 7, p. 1153, 2018, doi: [10.3390/rs10071153](https://doi.org/10.3390/rs10071153).
- [62] Z. Xu, G. Zheng, and L. M. Moskal, "Stratifying forest overstory for improving effective LAI estimation based on aerial imagery and discrete laser scanning data," *Remote Sens.*, vol. 12, no. 13, p. 2126, Jul. 2020, doi: [10.3390/rs12132126](https://doi.org/10.3390/rs12132126).
- [63] F. Morsdorf, O. Frey, E. Meier, K. I. Itten, and B. Allgöwer, "Assessment of the influence of flying altitude and scan angle on biophysical vegetation products derived from airborne laser scanning," *Int. J. Remote Sens.*, vol. 29, no. 5, pp. 1387–1406, Mar. 2008, doi: [10.1080/01431160701736349](https://doi.org/10.1080/01431160701736349).
- [64] K. Calders, J. Armston, G. Newnham, M. Herold, and N. Goodwin, "Implications of sensor configuration and topography on vertical plant profiles derived from terrestrial LiDAR," *Agric. Forest Meteorol.*, vol. 194, pp. 104–117, Aug. 2014, doi: [10.1016/j.agrformet.2014.03.022](https://doi.org/10.1016/j.agrformet.2014.03.022).
- [65] W. Yang, W. Ni-Meister, and S. Lee, "Assessment of the impacts of surface topography, off-nadir pointing and vegetation structure on vegetation LiDAR waveforms using an extended geometric optical and radiative transfer model," *Remote Sens. Environ.*, vol. 115, no. 11, pp. 2810–2822, Nov. 2011, doi: [10.1016/j.rse.2010.02.021](https://doi.org/10.1016/j.rse.2010.02.021).
- [66] Y. Wang, W. Ni, G. Sun, H. Chi, Z. Zhang, and Z. Guo, "Slope-adaptive waveform metrics of large footprint LiDAR for estimation of forest aboveground biomass," *Remote Sens. Environ.*, vol. 224, pp. 386–400, Apr. 2019, doi: [10.1016/j.rse.2019.02.017](https://doi.org/10.1016/j.rse.2019.02.017).
- [67] A. Kuusk, "Leaf orientation measurement in a mixed hemiboreal broadleaf forest stand using terrestrial laser scanner," *Trees*, vol. 34, no. 2, pp. 371–380, Apr. 2020, doi: [10.1007/s00468-019-01922-6](https://doi.org/10.1007/s00468-019-01922-6).
- [68] G. Yan *et al.*, "Quantitative evaluation of leaf inclination angle distribution on leaf area index retrieval of coniferous canopies," *J. Remote Sens.*, vol. 2021, pp. 1–15, Apr. 2021, doi: [10.34133/2021/2708904](https://doi.org/10.34133/2021/2708904).
- [69] L. Wallace, A. Lucieer, C. Watson, and D. Turner, "Development of a UAV-LiDAR system with application to forest inventory," *Remote Sens.*, vol. 4, no. 6, pp. 1519–1543, 2012, doi: [10.3390/rs4061519](https://doi.org/10.3390/rs4061519).
- [70] A. Kuusk, "Canopy radiative transfer modeling," in *Comprehensive Remote Sensing*, vol. 3, 2017, pp. 9–22. [Online]. Available: <http://www2.geog.ucl.ac.uk/~mdisney/teaching/GEOGG141/papers/kuuskRT.pdf>, doi: [10.1016/B978-0-12-409548-9.10534-2](https://doi.org/10.1016/B978-0-12-409548-9.10534-2).
- [71] J.-P. Gastellu-Etchegorry *et al.*, "Simulation of satellite, airborne and terrestrial LiDAR with DART (I): Waveform simulation with quasi-Monte Carlo ray tracing," *Remote Sens. Environ.*, vol. 184, pp. 418–435, Oct. 2016, doi: [10.1016/j.rse.2016.07.010](https://doi.org/10.1016/j.rse.2016.07.010).
- [72] G. Schaepmanstrub, M. E. Schaepman, T. H. Painter, S. Dangel, and J. Martonchik, "Reflectance quantities in optical remote sensing—definitions and case studies," *Remote Sens. Environ.*, vol. 103, no. 1, pp. 27–42, 2006, doi: [10.1016/j.rse.2006.03.002](https://doi.org/10.1016/j.rse.2006.03.002).
- [73] W. Qin, N. S. Goel, and B. Wang, "The hotspot effect in heterogeneous vegetation canopies and performances of various hotspot models," *Remote Sens. Rev.*, vol. 14, no. 4, pp. 283–332, Dec. 1996.



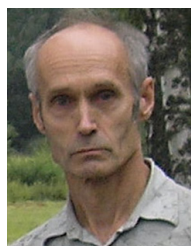
Shiyu Cheng received the M.Sc. degree in mapping and geography information systems from Beijing Normal University, Beijing, China, in 2021.

Her research interests include leaf area index estimation, clumping effect correction, and terrestrial laser scanning.



Guangjian Yan (Senior Member, IEEE) received the Ph.D. degree from the Institute of Remote Sensing Applications, Chinese Academy of Sciences, Beijing, China, in 1999.

He is a Professor with the State Key Laboratory of Remote Sensing Science, Institute of Remote Sensing Science and Engineering, Faculty of Geographical Science, Beijing Normal University, Beijing. He has published more than 200 articles. His main research interests are multiangular remote sensing, vegetation remote sensing, radiation budgets, and scale effects in remote sensing.



Andres Kuusk received the Ph.D. degree in geophysics from the Main Geophysical Observatory, Leningrad, Soviet Union, in 1979, and the D.Sc. degree in geophysics from Tartu University, Tõravere, Estonia, in 1991.

He is a Counsellor with the Group of Vegetation Remote Sensing, Tartu Observatory, Faculty of Science and Technology, Tartu University. His research interests include radiative transfer in vegetation canopies and optical remote sensing.



Ronghai Hu received the Ph.D. degrees in geographical information system from Beijing Normal University, Beijing, China, and remote sensing from the ICube Laboratory, Centre National de la Recherche Scientifique (CNRS), University of Strasbourg, Strasbourg, Illkirch, France, in 2018.

He is a Lecturer with the College of Resources and Environment, University of Chinese Academy of Sciences, Beijing. His research interests include indirect measurement and airborne retrieval of leaf area index (LAI), remote sensing of vegetation, light detection and ranging (LiDAR), and scale effect on remote sensing.



Hailan Jiang received the M.Sc. degree in mapping and geography information systems from Lanzhou University, Lanzhou, China, in 2015. She is currently pursuing the Ph.D. degree with Beijing Normal University, Beijing, China. She is also a joint Ph.D. student with the Department of Geography, University of Zurich, Zürich, Switzerland.

Her research interest focuses on the estimation of vegetation structure from laser scanning data.



Yiyi Tong received the M.Sc. degree in mapping and geography information systems from Beijing Normal University, Beijing, China, in 2020.

Her research interests include the estimation of radiation budgets and the validation of remote sensing models in rugged terrains.



Xihan Mu received the Ph.D. degree in remote sensing from the School of Geography, Beijing Normal University, Beijing, China, in 2009.

He is an Associate Professor with the State Key Laboratory of Remote Sensing Science, Institute of Remote Sensing Science and Engineering, Faculty of Geographical Science, Beijing Normal University. His research interest focuses on multiangular remote sensing, especially in the retrieval/measurement of vegetation structural parameters.



Guoqing Zhou (Senior Member, IEEE) received the Ph.D. degree from Wuhan University, Wuhan, China, in 1994.

He is a Professor with the Guangxi Key Laboratory for Spatial Information and Geomatics, Guilin University of Technology, Guilin, China. His research interests include photogrammetry and remote sensing, especially in remote sensing image processing and interpretation.



Donghui Xie received the Ph.D. degree in remote sensing and geographic information systems from Beijing Normal University, Beijing, China, in 2005.

She is an Associate Professor with the State Key Laboratory of Remote Sensing Science, Institute of Remote Sensing Science and Engineering, Faculty of Geographical Science, Beijing Normal University. Her research interests include canopy radiative transfer modeling, biophysical parameter retrieval of vegetation, and remote sensing data fusion.



Wuming Zhang received the Ph.D. degree from Tsinghua University, Beijing, China, in 2004.

He is a Professor with the School of Geospatial Engineering and Science, Sun Yat-sen University, Zhuhai, China. His research interests include photogrammetry and remote sensing, especially light detection and ranging (LiDAR) point cloud processing and applications.



Felix Morsdorf received the Ph.D. degree and *venia legendi* in geography, with a specialization in light detection and ranging (LiDAR) remote sensing, from the University of Zurich, Zürich, Switzerland, in 2007 and 2021, respectively.

He is a Group Leader with the Department of Geography, University of Zurich. His group uses empirical and physical approaches to bridge the semantic gap between data and information in the context of laser scanning and vegetation structure.